Springer Ser Chem Sens Biosens (2006) 4: 3–44
DOI 10.1007/5346_013

Published online: 5 July 2006

Electromagnetic Theory of Surface Plasmons

Jiří Homola

Institute of Radio Engineering and Electronics, Prague, Czech Republic
homola@ure.cas.cz

1 Introduction 3

2 Theory of Planar Metal/Dielectric Waveguides 4
2.1 Surface Plasmons on Metal–Dielectric Waveguides 8
2.2 Surface Plasmons on Dielectric–Metal–Dielectric Waveguides 14

3 Surface Plasmons on Waveguides with a Perturbed Refractive Index Profile 19
3.1 Perturbed Surface Plasmons on Metal–Dielectric Waveguides 21
3.2 Perturbed Surface Plasmons on Dielectric–Metal–Dielectric Waveguides . . 24

4 Excitation of Surface Plasmons 26
4.1 Prism Coupling 26
4.2 Grating Coupling 35
4.3 Waveguide Coupling 41

5 Summary 43

References 43

Keywords Excitation of surface plasmons · Grating coupler · Guided mode · Optical waveguide · Prism coupler · Surface plasmons

1 Introduction

The first documented observation of surface plasmons dates back to 1902, when Wood illuminated a metallic diffraction grating with polychromatic light and noticed narrow dark bands in the spectrum of the diffracted light, which he referred as to anomalies [1]. Theoretical work by Fano [2] concluded that these anomalies were associated with the excitation of electromagnetic surface waves on the surface of the diffraction grating. In 1958 Thurbadar observed a large drop in reflectivity when illuminating thin metal films on a substrate [3], but did not link this effect to surface plasmons. In 1968 Otto explained Turbadar's results and demonstrated that the drop in the reflectivity in the attenuated total reflection method is due to the excitation of surface plasmons [4]. In the same year, Kretschmann and Raether reported excitation of surface plasmons in another configuration of the attenuated

total reflection method [5]. The pioneering work of Otto, Kretschmann, and Raether established a convenient method for the excitation of surface plasmons and their investigation, and introduced surface plasmons into modern optics (see, for example [6], and [7]). In the late 1970s, surface plasmons were first employed for the characterization of thin films [8] and the study of processes at metal boundaries [9].

In this chapter we present an electromagnetic theory of surface plasmons based on theoretical analysis of light propagation in planar metal/dielectric waveguides. The main characteristics of surface plasmons propagating along metal–dielectric and dielectric–metal–dielectric waveguides are introduced and methods for optical excitation of surface plasmons are discussed.

2 Theory of Planar Metal/Dielectric Waveguides

In this section, we present an electromagnetic theory of optical waveguides based on solving Maxwell's equations using the modal method [10–12]. In this approach, the electric and magnetic field vectors $\boldsymbol{E}$ and $\boldsymbol{H}$ are each expressed as a sum of field contributions, one part representing power that is guided along the waveguide, the remaining part representing power that is radiated from the waveguide [10]:

$$\boldsymbol{E}(\boldsymbol{r},t) = \boldsymbol{E}_{\mathrm{G}}(\boldsymbol{r},t) + \boldsymbol{E}_{\mathrm{R}}(\boldsymbol{r},t)\,, \tag{1}$$

$$\boldsymbol{H}(\boldsymbol{r},t) = \boldsymbol{H}_{\mathrm{G}}(\boldsymbol{r},t) + \boldsymbol{H}_{\mathrm{R}}(\boldsymbol{r},t)\,, \tag{2}$$

where subscript G and R denote the guided and radiation fields, $\boldsymbol{r}$ is space vector and t is time. The guided, or bound, portion can be expressed as a finite sum of guided modes:

$$\boldsymbol{E}_{\mathrm{G}}(\boldsymbol{r},t) = \sum_j \alpha_j \boldsymbol{E}_j(\boldsymbol{r},t)\,, \tag{3}$$

$$\boldsymbol{H}_{\mathrm{G}}(\boldsymbol{r},t) = \sum_j \alpha_j \boldsymbol{H}_j(\boldsymbol{r},t)\,, \tag{4}$$

where j is a mode number ($j = 1, 2, \ldots, M$) and α_j are modal amplitudes. The modal fields $\boldsymbol{E}_j(\boldsymbol{r},t)$ and $\boldsymbol{H}_j(\boldsymbol{r},t)$ are solutions to source-free Maxwell equations:

$$\nabla \times \boldsymbol{E}(\boldsymbol{r},t) + \mu \frac{\partial \boldsymbol{H}(\boldsymbol{r},t)}{\partial t} = 0\,, \tag{5}$$

$$\nabla \cdot \big(\mu \boldsymbol{H}(\boldsymbol{r},t)\big) = 0\,, \tag{6}$$

$$\nabla \times \boldsymbol{H}(\boldsymbol{r},t) - \varepsilon_0 \varepsilon(\boldsymbol{r}) \frac{\partial \boldsymbol{E}(\boldsymbol{r},t)}{\partial t} = 0\,, \tag{7}$$

$$\nabla \cdot \big(\varepsilon_0 \varepsilon(\boldsymbol{r}) \boldsymbol{E}(\boldsymbol{r},t)\big) = 0\,, \tag{8}$$

where μ is magnetic permeability, ε is relative permittivity (dielectric constant) of the medium, and ε_0 is the free-space permittivity. For non-magnetic materials, which commonly constitute an optical waveguide, the magnetic permeability μ is equal to the free-space permeability μ_0. Assuming a waveguide consisting of linear isotropic media, we can reduce Maxwell's (Eqs. 5–8) to the vector wave equations:

$$\Delta \boldsymbol{E}(\boldsymbol{r},t) - \varepsilon_0\varepsilon(\boldsymbol{r})\mu_0\frac{\partial^2 \boldsymbol{E}(\boldsymbol{r},t)}{\partial t^2} = \nabla\left(\boldsymbol{E}(\boldsymbol{r},t)\cdot\nabla\ln\varepsilon_0\varepsilon(\boldsymbol{r})\right)\,, \tag{9}$$

$$\Delta \boldsymbol{H}(\boldsymbol{r},t) - \varepsilon_0\varepsilon(\boldsymbol{r})\mu_0\frac{\partial^2 \boldsymbol{H}(\boldsymbol{r},t)}{\partial t^2} = (\nabla\times\boldsymbol{H})\times\left(\nabla\ln\varepsilon_0\varepsilon(\boldsymbol{r})\right)\,, \tag{10}$$

where the vector differential operators ∇ and Δ are defined as follows:

$$\nabla f = \frac{\delta f}{\delta x}\boldsymbol{x}_0 + \frac{\delta f}{\delta y}\boldsymbol{y}_0 + \frac{\delta f}{\delta z}\boldsymbol{z}_0\,, \tag{11}$$

$$\nabla\cdot\boldsymbol{A} = \frac{\delta A_x}{\delta x} + \frac{\delta A_y}{\delta y} + \frac{\delta A_z}{\delta z}\,, \tag{12}$$

$$\nabla\times\boldsymbol{A} = \left(\frac{\delta A_y}{\delta z} - \frac{\delta A_z}{\delta y}\right)\boldsymbol{x}_0 + \left(\frac{\delta A_z}{\delta x} - \frac{\delta A_x}{\delta z}\right)\boldsymbol{y}_0 + \left(\frac{\delta A_x}{\delta y} - \frac{\delta A_y}{\delta x}\right)\boldsymbol{z}_0\,, \tag{13}$$

$$\begin{aligned}\Delta\boldsymbol{A} = &\left(\frac{\partial^2 A_x}{\partial x^2} + \frac{\partial^2 A_x}{\partial y^2} + \frac{\partial^2 A_x}{\partial z^2}\right)\boldsymbol{x}_0 + \left(\frac{\partial^2 A_y}{\partial x^2} + \frac{\partial^2 A_y}{\partial y^2} + \frac{\partial^2 A_y}{\partial z^2}\right)\boldsymbol{y}_0\\ &+ \left(\frac{\partial^2 A_z}{\partial x^2} + \frac{\partial^2 A_z}{\partial y^2} + \frac{\partial^2 A_z}{\partial z^2}\right)\boldsymbol{z}_0\,,\end{aligned} \tag{14}$$

and f and $\boldsymbol{A} = (A_x, A_y, A_z)$ are scalar and vector functions on cartesian coordinates (x, y, z) and $\boldsymbol{x}_0$, $\boldsymbol{y}_0$ and $\boldsymbol{z}_0$ are unit vectors. If we assume translational invariance of the waveguide in the z-direction, propagation along the z-direction, and time dependence of the field vectors in the form of $\exp(-\mathrm{i}\omega t)$, where ω is the angular frequency and $\mathrm{i} = \sqrt{-1}$, the modal fields can be expressed in the separable form:

$$\boldsymbol{E} = \boldsymbol{e}(x,y)\exp\left(\mathrm{i}(\beta z - \omega t)\right) = \left\{\boldsymbol{e}_\mathrm{t}(x,y) + e_z(x,y)\boldsymbol{z}_0\right\}\exp\left(\mathrm{i}(\beta z - \omega t)\right)\,, \tag{15}$$

$$\boldsymbol{H} = \boldsymbol{h}(x,y)\exp\left(\mathrm{i}(\beta z - \omega t)\right) = \left\{\boldsymbol{h}_\mathrm{t}(x,y) + h_z(x,y)\boldsymbol{z}_0\right\}\exp\left(\mathrm{i}(\beta z - \omega t)\right)\,, \tag{16}$$

where β denotes the propagation constant of a mode and subscript t denotes the transversal component of field vectors. For the modal fields described by Eqs. 15 and 16, the vector wave equations can be reduced to:

$$\left\{\Delta_\mathrm{t} + \omega^2\varepsilon\varepsilon_0\mu_0 - \beta^2\right\}\boldsymbol{e} = -\left\{\nabla_t + \mathrm{i}\beta\boldsymbol{z}\right\}\left\{\boldsymbol{e}_\mathrm{t}\nabla_\mathrm{t}\ln\varepsilon\varepsilon_0\right\}\,, \tag{17}$$

$$\left\{\Delta_\mathrm{t} + \omega^2\varepsilon\varepsilon_0\mu_0 - \beta^2\right\}\boldsymbol{h} = -\left(\nabla_\mathrm{t}\ln\varepsilon\varepsilon_0\right)\times\left(\left\{\nabla_\mathrm{t} + \mathrm{i}\beta\boldsymbol{z}\right\}\times\boldsymbol{h}\right)\,. \tag{18}$$

These vector wave equations are a restatement of Maxwell's equations for an arbitrary refractive index profile. Subject to the requirements that the modal fields are bounded everywhere and decay sufficiently fast at large distances from the waveguide, these equations contain all of the information necessary to determine the modal fields and propagation constants of all the guided modes of the waveguide.

Let us consider an optical waveguide consisting of three homogeneous media (Fig. 1) with a permittivity profile:

$$\varepsilon(x) = \varepsilon_3 = n_3^2\,, \quad x > d\,, \tag{19}$$

$$\varepsilon(x) = \varepsilon_2 = n_2^2\,, \quad -d \leq x \leq d\,, \tag{20}$$

$$\varepsilon(x) = \varepsilon_1 = n_1^2\,, \quad x < -d\,, \tag{21}$$

where d is the waveguiding layer half-width and ε_i and n_i ($i = 1, 2, 3$) are generally complex permittivities and refractive indices (hereafter, we shall be using ε for the *relative* permittivity unless stated otherwise).

By orienting cartesian axes as shown in Fig. 1, the field vectors depend on x and z only and Eqs. 15 and 16 can be written as:

$$\boldsymbol{E} = \boldsymbol{e}(x)\exp\left(\mathrm{i}(\beta z - \omega t)\right)\,, \tag{22}$$

$$\boldsymbol{H} = \boldsymbol{h}(x)\exp\left(\mathrm{i}(\beta z - \omega t)\right)\,, \tag{23}$$

In each medium the $\nabla_\mathrm{t} \ln \varepsilon$ term vanishes and each cartesian field component satisfies a simplified wave equation:

$$\left\{\Delta_\mathrm{t} + \omega^2 \varepsilon \varepsilon_0 \mu_0 - \beta^2\right\} e_i = 0\,, \tag{24}$$

$$\left\{\Delta_\mathrm{t} + \omega^2 \varepsilon \varepsilon_0 \mu_0 - \beta^2\right\} h_i = 0\,, \tag{25}$$

where $i = x, y, z$.

The solution of Eqs. 24 and 25 yields two linearly independent sets of modes. One set with $h_z = 0$ everywhere, referred as to transverse magnetic (TM); the other with $e_z = 0$ everywhere, referred as to transverse electric (TE). Substitution of the field profiles Eqs. 22 and 23 into Eqs. 24 and 25, respec-

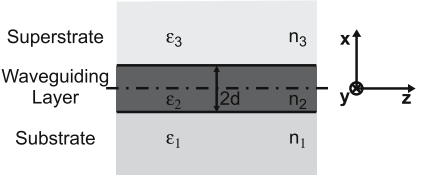

Fig. 1 Section of a planar waveguide with a step refractive index profile

tively, yields for the transversal components of the field vectors:

$$\frac{\partial^2 e_y(x)}{\partial x^2} + (\omega^2 \varepsilon \varepsilon_0 \mu_0 - \beta^2) e_y(x) = 0\,; \quad \text{for the TE modes}\,, \tag{26}$$

$$\frac{\partial^2 h_y(x)}{\partial x^2} + (\omega^2 \varepsilon \varepsilon_0 \mu_0 - \beta^2) h_y(x) = 0\,; \quad \text{for the TM modes}\,. \tag{27}$$

In each medium the solution of wave Eqs. 26 and 27 can be expressed as a linear combination of functions: $\exp(\mathrm{i}\kappa_i x)$ and $\exp(-\mathrm{i}\kappa_i x)$, where $\kappa_i^2 = \omega^2 \varepsilon_i \varepsilon_0 \mu_0 - \beta^2$ $(i = 1, 2, 3)$. The other non-zero components of the field vectors can be determined from Eqs. 5 and 7. This yields:

$$\underline{\text{TE modes:}} \quad e_y(x) = a_i^+ \exp(\mathrm{i}\kappa_i x) + a_i^- \exp(-\mathrm{i}\kappa_i x)\,, \tag{28}$$

$$h_x(x) = \frac{\beta}{\mu_0 \omega} \left[a_i^+ \exp(\mathrm{i}\kappa_i x) + a_i^- \exp(-\mathrm{i}\kappa_i x) \right]\,, \tag{29}$$

$$h_z(x) = -\frac{\kappa_i}{\mu_0 \omega} \left[a_i^+ \exp(\mathrm{i}\kappa_i x) - a_i^- \exp(-\mathrm{i}\kappa_i x) \right]\,, \text{ and} \tag{30}$$

$$\underline{\text{TM modes:}} \quad h_y(x) = b_i^+ \exp(\mathrm{i}\kappa_i x) + b_i^- \exp(-\mathrm{i}\kappa_i x)\,, \tag{31}$$

$$e_x(x) = -\frac{\beta}{\varepsilon_i \varepsilon_0 \omega} \left[b_i^+ \exp(\mathrm{i}\kappa_i x) + b_i^- \exp(-\mathrm{i}\kappa_i x) \right]\,, \tag{32}$$

$$e_z(x) = \frac{\kappa_i}{\varepsilon_i \varepsilon_0 \omega} \left[b_i^+ \exp(\mathrm{i}\kappa_i x) - b_i^- \exp(-\mathrm{i}\kappa_i x) \right]\,. \tag{33}$$

Outside the waveguiding layer, modal fields bound to the waveguide are described by only one of these solutions and decay exponentially with an increasing distance from the waveguide. Consequently, in each pair of amplitudes a_1^+ and a_1^- and a_3^+ and a_3^-, one amplitude is equal to zero for TE modes, and in each pair of amplitudes b_1^+ and b_1^- and b_3^+ and b_3^-, one amplitude is equal to zero for TM modes. The boundary conditions of Maxwell's equations require that the components of the electric and magnetic field intensity vectors parallel to the boundaries of the waveguiding layer are continuous at the boundaries ($x = d$ and $x = -d$). These boundary conditions present a homogenous series of four linear equations for four unknown amplitudes, which yields a non-zero solution only if the determinant of the matrix of coefficients is equal to zero. This requirement leads to the eigenvalue equations:

$$\tan(\kappa d) = \frac{\gamma_1/\kappa + \gamma_3/\kappa}{1 - (\gamma_1/\kappa)(\gamma_3/\kappa)}\,; \text{ for the TE modes}\,, \tag{34}$$

$$\tan(\kappa d) = \frac{\gamma_1 \varepsilon_2/\kappa\varepsilon_1 + \gamma_3 \varepsilon_2/\kappa\varepsilon_3}{1 - (\gamma_1 \varepsilon_2/\kappa\varepsilon_1)(\gamma_3 \varepsilon_2/\kappa\varepsilon_3)}\,; \text{ for the TM modes}\,, \tag{35}$$

where $\kappa^2 = \omega^2 \varepsilon_2 \varepsilon_0 \mu_0 - \beta^2$ and $\gamma_{1,3}^2 = \beta^2 - \omega^2 \varepsilon_{1,3} \varepsilon_0 \mu_0$.

The eigenvalue Eqs. 34 and 35 are transcendental equations for unknown modal propagation constants. After solving the eigenvalue equations, the field profiles can be determined by substituting the values of modal propagation constants β into the boundary conditions and calculating the amplitudes a_i^+ and a_i^- for TE modes and b_i^+ and b_i^- for TM modes ($i = 1, 2, 3$).

If the media constituting the waveguide are lossless ($\varepsilon_1, \varepsilon_2$, and ε_3 are real positive numbers), the propagation constants are also real. Propagation constants of modes of a waveguide containing absorbing media (e.g., metal) are complex. The propagation constant is related to the modal effective index n_{ef} and modal attenuation b as follows:

$$n_{\mathrm{ef}} = \frac{c}{\omega} \mathrm{Re}\{\beta\} \,, \tag{36}$$

$$b = \mathrm{Im}\{\beta\} \frac{0.2}{\ln 10} \,, \tag{37}$$

where Re{} and Im{} denote the real and imaginary parts of a complex number, respectively, and c denotes the speed of light in vacuum; the modal attenuation b is in dB cm^{-1} if β is given in m^{-1}.

2.1 Surface Plasmons on Metal–Dielectric Waveguides

A waveguide consisting of a semi-infinite metal with a complex permittivity $\varepsilon_{\mathrm{m}} = \varepsilon'_{\mathrm{m}} + \mathrm{i}\varepsilon''_{\mathrm{m}}$, and a semi-infinite dielectric with permittivity $\varepsilon_{\mathrm{d}} = \varepsilon'_{\mathrm{d}} + \mathrm{i}\varepsilon''_{\mathrm{d}}$, where ε'_i and ε''_i are real and imaginary parts of ε_i (i is m or d), see Fig. 2, can be treated as a limiting case of a three-layer waveguide (Fig. 1) with a metal substrate, a dielectric superstrate, and a waveguiding layer with a thickness equal to zero.

The propagation constants of the guided modes propagating along such a structure are the solutions of Eqs. 34 and 35, which for $d = 0$ can be rewritten as:

$$\gamma_{\mathrm{m}} = -\gamma_{\mathrm{d}} \,; \quad \text{for the TE modes} \,, \tag{38}$$

$$\frac{\gamma_{\mathrm{m}}}{\varepsilon_{\mathrm{m}}} = -\frac{\gamma_{\mathrm{d}}}{\varepsilon_{\mathrm{d}}} \,; \quad \text{for the TM modes} \,, \tag{39}$$

where $\gamma_i^2 = \beta^2 - \omega^2 \mu_0 \varepsilon_0 \varepsilon_i$ (i is m or d). The eigenvalue equation for TE modes (1.38) yields no solution that would represent a bounded mode. The TM

Fig. 2 A metal–dielectric waveguide

mode eigenvalue (Eq. 39) can be reduced to:

$$\beta = \frac{\omega}{c}\sqrt{\frac{\varepsilon_\mathrm{d}\varepsilon_\mathrm{m}}{\varepsilon_\mathrm{d}+\varepsilon_\mathrm{m}}} = k\sqrt{\frac{\varepsilon_\mathrm{d}\varepsilon_\mathrm{m}}{\varepsilon_\mathrm{d}+\varepsilon_\mathrm{m}}}\,, \tag{40}$$

where c is the speed of light in vacuum and $k = 2\pi/\lambda$ is the free-space wavenumber, where λ is the free-space wavelength [6, 7]. For lossless metal and dielectric ($\varepsilon''_\mathrm{m} = \varepsilon''_\mathrm{d} = 0$), Eqs. 39 and 40 represent a guided mode, providing that the permittivities ε'_m and ε'_d are of opposite signs, and that $\varepsilon'_\mathrm{m} < -\varepsilon'_\mathrm{d}$. This guided mode is sometimes referred as to the Fano mode [7]. As the permittivity of dielectric materials is usually positive, for the Fano mode to exist, the real part of the permittivity of the metal needs to be negative. For metals following the free-electron model [13]:

$$\varepsilon_\mathrm{m} = \varepsilon_0\left(1 - \frac{\omega_\mathrm{p}^2}{\omega^2 + \mathrm{i}\omega\nu}\right)\,, \tag{41}$$

where ν is the collision frequency and ω_p is the plasma frequency:

$$\omega_\mathrm{p} = \sqrt{\frac{Ne^2}{\varepsilon_0 m_\mathrm{e}}}\,, \tag{42}$$

where N is the concentration of free electrons, and e and m_e are the electron charge and mass, respectively, this requirement is fulfilled for frequencies lower than the plasma frequency of the metal. As shown in Fig. 3 metals such as gold, silver and aluminum exhibit a negative real part of permittivity in visible and near infrared region of the spectrum.

Absorption, which in reality always exists, introduces a non-zero imaginary part into the permittivity of metals (Fig. 3, lower plot) and permits the existence of guided modes even for $\varepsilon'_\mathrm{m} > -\varepsilon_\mathrm{d}$. These modes, sometimes referred as to evanescent modes [7], exhibit a very high attenuation and are therefore less practically important. In this work, we shall refer to all of the guided modes described by eigenvalue (Eq. 40) as *surface plasmons* (SP).

If the real part of the permittivity of the metal is negative and its magnitude is much larger than the imaginary part $\left|\varepsilon'_\mathrm{m}\right| \gg \varepsilon''_\mathrm{m}$, the complex propagation constant of the surface plasmon given by Eq. 40 can be expressed as:

$$\beta = \beta' + \mathrm{i}\beta'' \doteq \frac{\omega}{c}\sqrt{\frac{\varepsilon'_\mathrm{m}\varepsilon_\mathrm{d}}{\varepsilon'_\mathrm{m}+\varepsilon_\mathrm{d}}} + \mathrm{i}\frac{\varepsilon''_\mathrm{m}}{2(\varepsilon'_\mathrm{m})^2}\frac{\omega}{c}\left(\frac{\varepsilon'_\mathrm{m}\varepsilon_\mathrm{d}}{\varepsilon'_\mathrm{m}+\varepsilon_\mathrm{d}}\right)^{3/2}\,, \tag{43}$$

where β' and β'' denote the real and imaginary parts of the propagation constant β [6]. As follows from Eq. 43, the imaginary part of the permittivity of metal ε''_m causes the propagation constant of a surface plasmon to have a non-zero imaginary part, which is associated with attenuation of the surface plasmon. The attenuation is sometimes characterized by the propagation length L, which is defined as the distance in the direction of propagation at

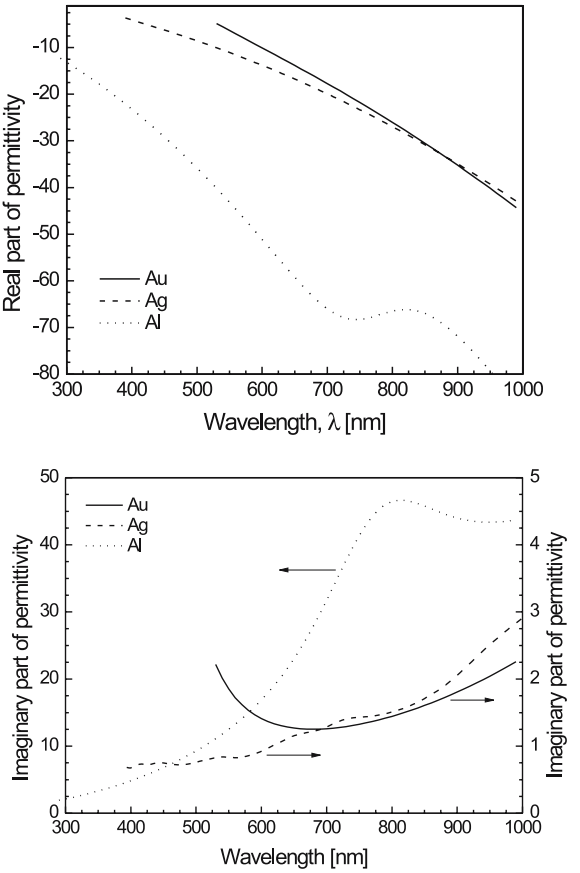

Fig. 3 Permittivity of gold, silver and aluminum as a function of wavelength. Real part of permittivity (*upper plot*) and imaginary part of permittivity (*lower plot*). Data determined ellipsometrically or taken from [14]

which the energy of the surface plasmon decreases by a factor of 1/e:

$$L = 1/\left[2\beta''\right] . \tag{44}$$

Spectral dependencies of the effective index, attenuation, and propagation length of a surface plasmon supported by gold, silver and aluminum are shown in Fig. 4.

As follows from Fig. 4, the existence of a surface plasmon on a metal–dielectric interface is confined to wavelengths longer than a certain critical wavelength, which depends on the plasma frequency and is specific to the metal. For metals such as gold, silver, and aluminum this critical wavelength lies in the UV or visible region. The effective index of a surface plasmon is larger than the effective index of a light wave in the dielectric medium and decreases with increasing wavelength. Attenuation of a surface plasmon

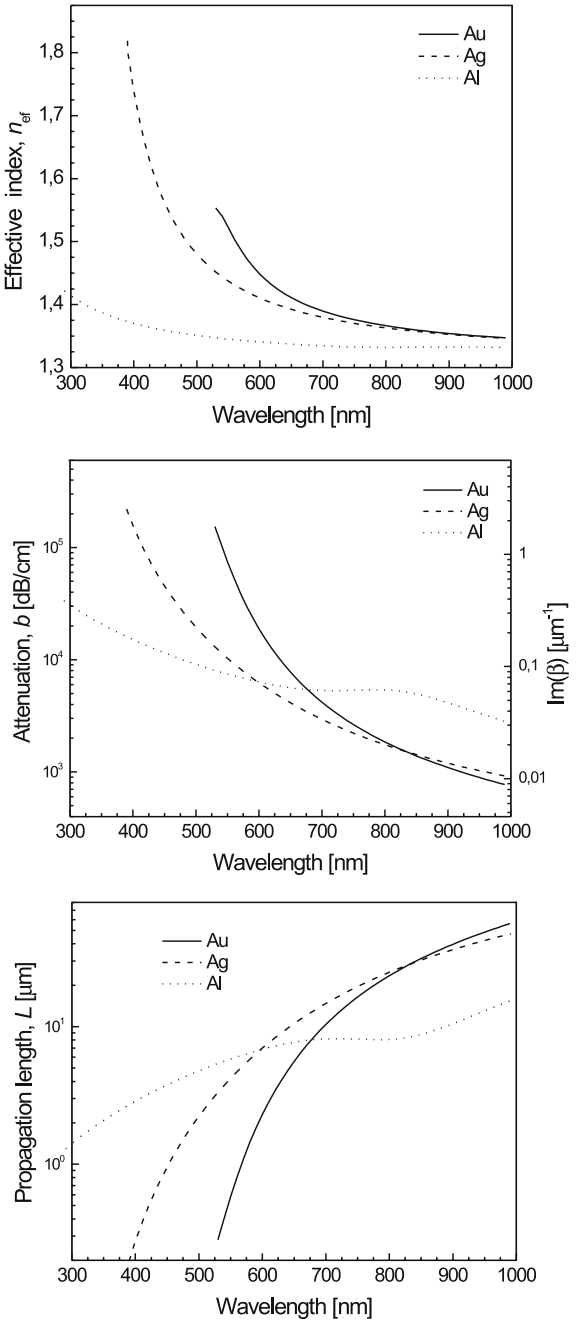

Fig. 4 Effective index, attenuation and propagation length of a surface plasmon propagating along the interface between a dielectric (refractive index 1.32) and a metal as a function of wavelength calculated for gold (Au), silver (Ag), and aluminum (Al)

follows the same trend. As the attenuation of a surface plasmon is proportional to $\varepsilon''_m/\varepsilon'^2_m$, the effect of the imaginary part of the permittivity of the metal can be outweighed by the real part of the permittivity. For instance, aluminum exhibits a much larger imaginary part of permittivity than silver. However, the surface plasmons on silver and aluminum suffer approximately the same attenuation at a wavelength of 600 nm as the real part of the permittivity of aluminum is much larger than that of silver. In the wavelength range 550–1000 nm, typical propagation lengths of surface plasmons are 0.6–50 μm, 4–50 μm, and 6–14 μm, for gold, silver and aluminum, respectively.

The distribution of electric and magnetic intensity vectors of a surface plasmon can be obtained from Eqs. 31–33:

$$h_y(x) = A\exp(\gamma_m x) \quad \text{for} \quad x < 0 \quad \text{and}$$
$$h_y(x) = A\exp(-\gamma_d x) \quad \text{for} \quad x > 0 \tag{45}$$

$$e_x(x) = A\frac{\beta}{\omega\varepsilon_m\varepsilon_0}\exp(\gamma_m x) \quad \text{for} \quad x < 0 \quad \text{and}$$
$$e_x(x) = A\frac{\beta}{\omega\varepsilon_d\varepsilon_0}\exp(-\gamma_d x) \quad \text{for} \quad x > 0 \tag{46}$$

$$e_z(x) = A\frac{\gamma_m}{\omega\varepsilon_m\varepsilon_0}\exp(\gamma_m x) \quad \text{for} \quad x < 0 \quad \text{and}$$
$$e_z(x) = -A\frac{\gamma_d}{\omega\varepsilon_d\varepsilon_0}\exp(-\gamma_d x) \quad \text{for} \quad x > 0\,, \tag{47}$$

where:

$$\gamma_m = ik\frac{\varepsilon_m}{\sqrt{\varepsilon_m + \varepsilon_d}} \quad \text{and} \quad \gamma_d = ik\frac{\varepsilon_d}{\sqrt{\varepsilon_m + \varepsilon_d}}\,, \tag{48}$$

and the signs of the square roots in Eq. 48 are chosen so that the real parts of γ_m and γ_d are positive. A denotes the modal field amplitude.

As follows from Fig. 5, the electromagnetic field of a surface plasmon reaches its maximum at the metal–dielectric interface and decays into both media. The field decay in the direction perpendicular to the metal–dielectric interface is characterized by the penetration depth L_p, which is defined as the distance from the interface at which the amplitude of the field decreases by a factor of 1/e:

$$L_{pm} = 1/\,\mathrm{Re}\{\gamma_m\} \quad \text{and} \quad L_{pd} = 1/\,\mathrm{Re}\{\gamma_d\} \tag{49}$$

The spectral dependence of the penetration depth of a surface plasmon at the interface between gold and a non-dispersive medium with a refractive index of 1.32 is shown in Fig. 6. As follows from Fig. 6, with an increasing wavelength, the portion of the electromagnetic field carried in the dielectric increases and the field of the surface plasmon extends farther into the dielectric.

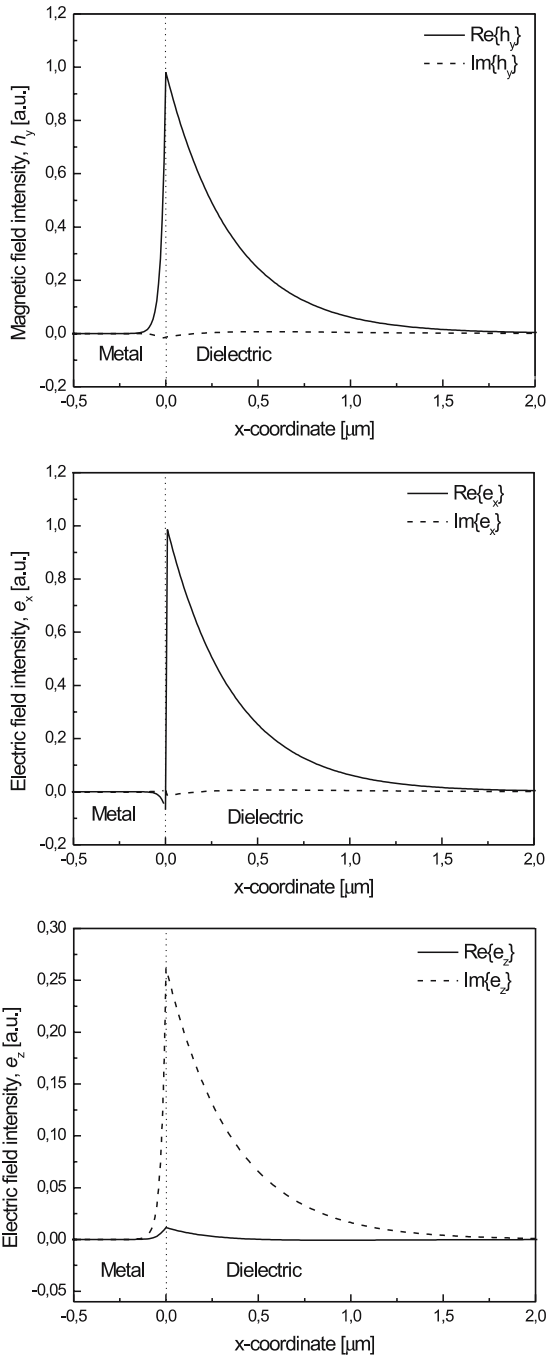

Fig. 5 Distribution of electric and magnetic field of a surface plasmon at the interface of gold ($\varepsilon_m = -25 + 1.44i$) and dielectric (refractive index 1.32), wavelength 800 nm

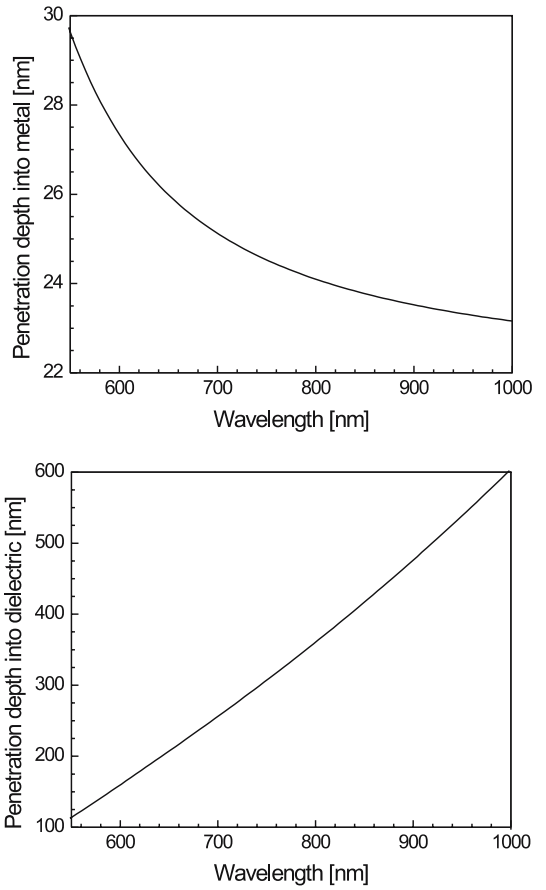

Fig. 6 Penetration depth of a surface plasmon into the metal (*upper plot*) and dielectric (*lower plot*) as a function of wavelength for a surface plasmon propagating along the interface of gold and a dielectric (refractive index 1.32)

2.2 Surface Plasmons on Dielectric–Metal–Dielectric Waveguides

Another example of a planar waveguide supporting surface plasmons is a thin metal film sandwiched between two semi-infinite dielectric media (Fig. 7). If the metal film is much thicker than the penetration depth of a surface plasmon at each metal–dielectric interface, this waveguide supports two TM modes, which correspond to two surface plasmons at the opposite boundaries of the metal film. When the metal thickness decreases, coupling between the two surface plasmons occurs, giving rise to mixed modes of electromagnetic field.

The modes of a dielectric–metal–dielectric waveguide can be found by solving the eigenvalue (Eq. 35). Numerical solutions of this eigenvalue equation for a symmetric waveguide structure ($n_{d1} = n_{d2}$) are shown in Fig. 8. For any thickness of the metal film, there are two coupled surface plasmons, which are referred as to the symmetric and antisymmetric surface plasmons,

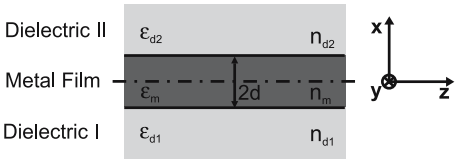

Fig. 7 Thin metal layer sandwiched between two dielectrics

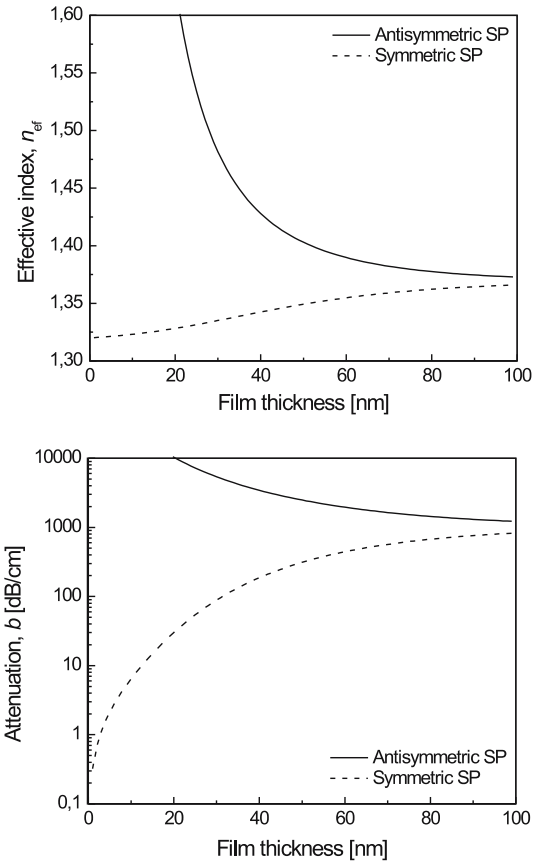

Fig. 8 Effective index and modal attenuation of surface plasmons propagating along a thin gold film ($\varepsilon_m = -25 + 1.44i$) sandwiched between two identical dielectrics ($n_{d1} = n_{d2} = 1.32$) as a function of the thickness of the gold film; wavelength 800 nm

based on the symmetry of the magnetic intensity distribution [14, 15]. The symmetric surface plasmon exhibits effective index and attenuation, which both increase with an increasing metal film thickness. The effective index and attenuation of the antisymmetric surface plasmon decrease with an increasing thickness of the metal film. If the waveguide is asymmetric, the effective index of the symmetric surface plasmon decreases with a decreasing metal film thickness and at a certain metal film thickness, the symmetric surface plasmon ceases to exist as a guided mode, Fig. 9, (this phenomenon is referred as to the mode cut-off). The symmetric surface plasmon exhibits a lower attenuation than its antisymmetric counterpart and therefore it is sometimes referred as to a long-range surface plasmon [16], while the antisymmetric mode is referred as to a short-range surface plasmon [14, 15].

Figures 10 and 11 show the field vector profiles of the symmetric and antisymmetric surface plasmons on a thin gold film surrounded by two identical dielectrics. The profiles of magnetic intensity h_y of symmetric and antisymmetric plasmons are symmetric or antisymmetric with respect to the center

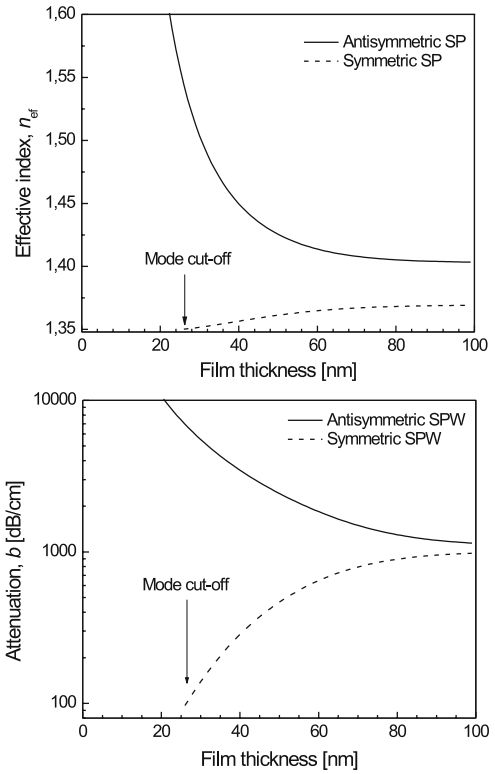

Fig. 9 Effective index and modal attenuation of surface plasmons propagating along a thin gold film ($\varepsilon_m = -25 + 1.44i$) sandwiched between two dielectrics ($n_{d1} = 1.32$ and $n_{d2} = 1.35$) as a function of the thickness of the gold film; wavelength 800 nm

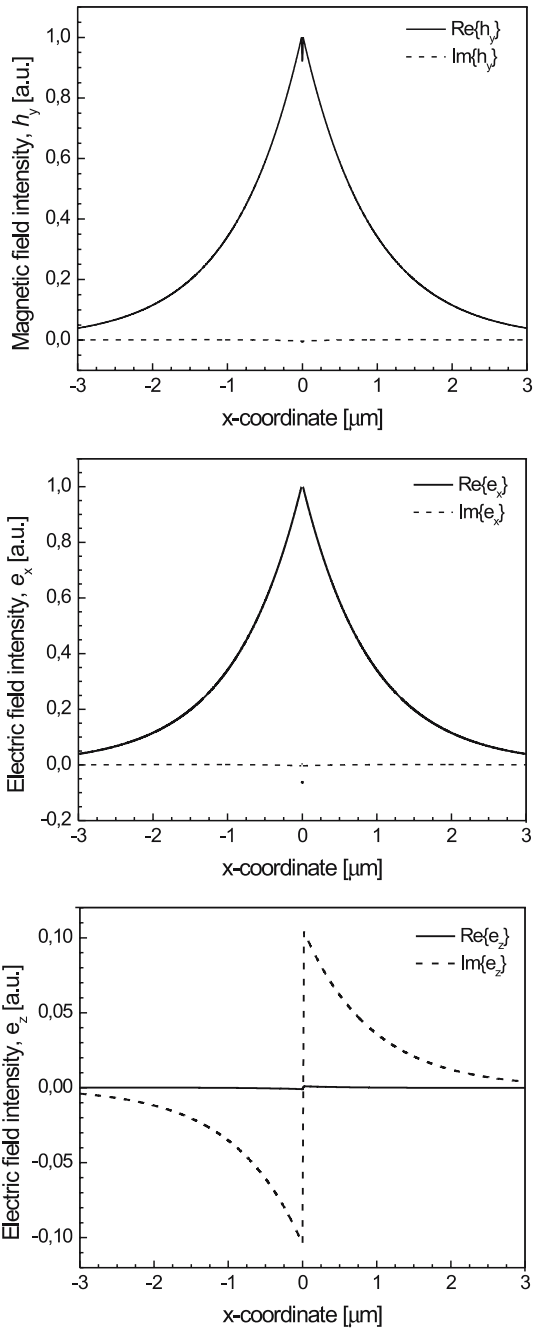

Fig. 10 Field profile of a symmetric surface plasmon on a thin gold film ($\varepsilon_m = -25 + 1.44i$) sandwiched between two identical dielectrics ($n_{d1} = n_{d2} = 1.32$), thickness of the gold film 20 nm, wavelength 800 nm

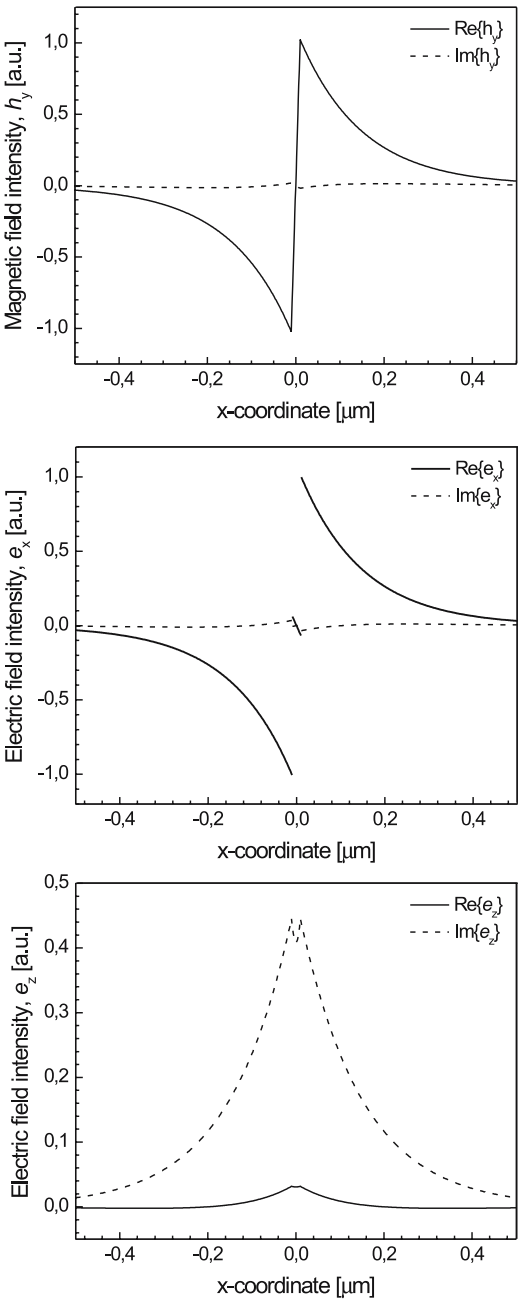

Fig. 11 Field profile of an antisymmetric surface plasmon on a thin gold film ($\varepsilon_m = -25 + 1.44i$) sandwiched between two identical dielectrics ($n_{d1} = n_{d2} = 1.32$), thickness of the gold film 20 nm, wavelength 800 nm

of the metal. The field of the symmetric surface plasmon penetrates deeper into the dielectric media than that of the antisymmetric surface plasmon.

3 Surface Plasmons on Waveguides with a Perturbed Refractive Index Profile

Surface plasmons are characterized by a (complex) propagation constant and a distribution of their electromagnetic field. The propagation constant is a solution of an appropriate eigenvalue equation and depends on the refractive index profile of the waveguide and angular frequency of surface plasmon. If the refractive index profile of the waveguide is perturbed, the propagation constant of the surface plasmon changes. The relationship between the change in the propagation constant of a surface plasmon and a perturbation in the refractive index profile can be analyzed using the perturbation theory [10].

In the perturbation theory, we assume that the magnetic field vector h_y of a surface plasmon supported by a general planar waveguide with and without the refractive index profile perturbation is described by Eq. 18. For the unperturbed and perturbed waveguide with permittivity profiles $\varepsilon(x)$ and $\bar{\varepsilon}(x) = \varepsilon(x) + \delta\varepsilon(x)$, respectively, this equation can be rewritten as:

$$\left\{\frac{\partial^2}{\partial x^2} + \omega^2\varepsilon\mu - \beta^2\right\} h_y = \frac{\partial \ln\varepsilon}{\partial x}\frac{\partial}{\partial x}h_y \quad \text{for the unperturbed waveguide, and} \tag{50}$$

$$\left\{\frac{\partial^2}{\partial x^2} + \omega^2\overline{\varepsilon}\mu - \overline{\beta}^2\right\} \overline{h}_y = \frac{\partial \ln\overline{\varepsilon}}{\partial x}\frac{\partial}{\partial x}\overline{h}_y \quad \text{for the unperturbed waveguide,} \tag{51}$$

where $\overline{\beta}$ and $\overline{h}_y$ denote the perturbed modal propagation constant and modal field, respectively. If we multiply Eq. 50 with $\overline{h}_y/\bar{\varepsilon}$, Eq. 51 with h_y/ε, subtract the two equations, and integrate the resulting equation over the cross-section of the waveguide A_∞, we obtain [17]:

$$\beta^2 - \overline{\beta}^2 = \frac{\beta^2 \int\limits_{A_\infty} \left(\frac{1}{\bar{\varepsilon}} - \frac{1}{\varepsilon}\right) h_y\bar{h}_y \,\mathrm{d}A + \int\limits_{A_\infty} \left(\frac{1}{\bar{\varepsilon}} - \frac{1}{\varepsilon}\right) \frac{\partial h_y}{\partial x}\frac{\partial \bar{h}_y}{\partial x} \,\mathrm{d}A}{\int\limits_{A_\infty} \frac{1}{\bar{\varepsilon}} h_y\bar{h}_y \,\mathrm{d}A}. \tag{52}$$

For a small permittivity profile perturbation $|\delta\varepsilon(x)| \ll |\varepsilon(x)|$, we can assume that the modal field remains unchanged ($h_y \doteq \bar{h}_y$) and the modal propagation constant is altered only slightly ($\left|\beta - \overline{\beta}\right| \ll |\beta|$). Then, Eq. 52 can be reduced

to:

$$\delta\beta = \frac{\beta^2 \int\limits_{A_\infty} \frac{\delta\varepsilon}{\varepsilon^2} h_y^2 \, \mathrm{d}A + \int\limits_{A_\infty} \frac{\delta\varepsilon}{\varepsilon^2} \left(\frac{\partial h_y}{\partial x}\right)^2 \mathrm{d}A}{2\beta \int\limits_{A_\infty} \frac{1}{\varepsilon} h_y^2 \, \mathrm{d}A} . \tag{53}$$

Furthermore, we shall apply this perturbation formula to the investigation of the effect of selected types of refractive index changes on (a) surface plasmons propagating along a single metal–dielectric interface (metal–dielectric waveguide) and (b) coupled surface plasmons propagating along a thin metal film (dielectric–metal–dielectric waveguide), Fig. 12.

Two main types of refractive index perturbations will be discussed here in detail. The first type is a homogeneous change in the refractive index in the whole superstrate, Fig. 13, (herein referred as to bulk refractive index change), which can be described by a change in the permittivity profile, $\varepsilon(x) \to \bar{\varepsilon}(x)$, where:

$$\varepsilon(x) = \begin{cases} \varepsilon_\mathrm{d} \\ \varepsilon_\mathrm{m} \end{cases} \quad \text{and} \quad \bar{\varepsilon}(x) = \begin{cases} \varepsilon_\mathrm{d} + \delta\varepsilon \\ \varepsilon_\mathrm{m} \end{cases} \quad \text{for} \quad \begin{matrix} x > 0 \\ x \leq 0 \end{matrix} . \tag{54}$$

The second type of perturbation is a homogenous change in the refractive index that occurs within a limited distance h from the surface of the metal film which is smaller than the penetration depth of a surface plasmon, Fig. 14, (herein referred as to surface refractive index change). Such a refractive index perturbation is characterized by a permittivity profile change $\varepsilon(x) \to \bar{\varepsilon}(x)$, where:

$$\varepsilon(x) = \begin{cases} \varepsilon_\mathrm{d} \\ \varepsilon_\mathrm{d} \\ \varepsilon_\mathrm{m} \end{cases} \quad \text{and} \quad \bar{\varepsilon}(x) = \begin{cases} \varepsilon_\mathrm{d} \\ \varepsilon_\mathrm{d} + \delta\varepsilon \\ \varepsilon_\mathrm{m} \end{cases} \quad \text{for} \quad \begin{matrix} x \geq h \\ 0 < x < h \\ x \leq 0 \end{matrix} , \tag{55}$$

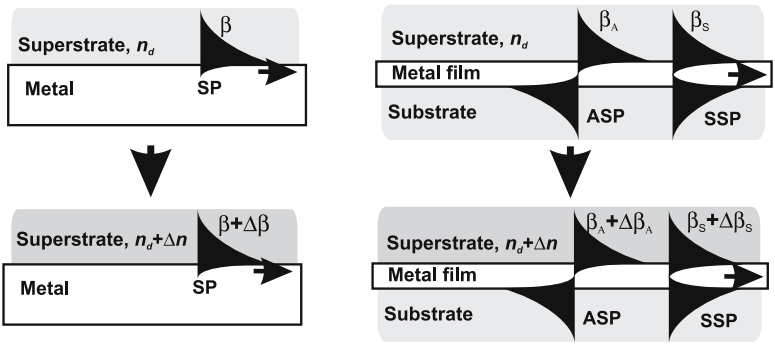

Fig. 12 Surface plasmons on a metal–dielectric waveguide (*left*) and a dielectric–metal–dielectric waveguide (*right*) with a perturbed refractive index of superstrate

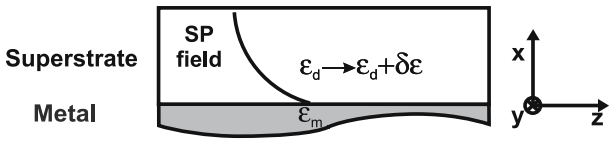

Fig. 13 Refractive index change occurring within a whole superstrate

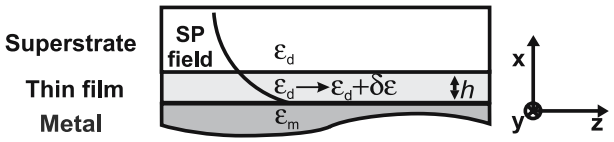

Fig. 14 A homogeneous refractive index change occurring within a short distance from the metal surface

3.1 Perturbed Surface Plasmons on Metal–Dielectric Waveguides

A change in the propagation constant of a surface plasmon on a metal–dielectric interface produced by a bulk refractive index change can be calculated by substituting the perturbation of the permittivity profile (Eq. 54) and the field distribution of the surface plasmon (Eq. 48) into the perturbation formula (Eq. 53). After a straightforward manipulation, the following analytical expressions for the perturbations in the propagation constant $\delta\beta$, and the effective refractive index δn_{ef} can be obtained:

$$\delta\beta = \frac{\beta^3}{2k^2\varepsilon_{\mathrm{d}}^2}\delta\varepsilon = \frac{\beta^3}{k^2 n_{\mathrm{d}}^3}\delta n\,, \tag{56}$$

$$\delta n_{\mathrm{ef}} = \frac{n_{\mathrm{ef}}^3}{n_{\mathrm{d}}^3}\delta n\,. \tag{57}$$

where the perturbation in the refractive index and permittivity are related as $\delta\varepsilon = 2n_{\mathrm{d}}\delta n$. As the effective index of the surface plasmon at a metal–dielectric interface n_{ef} is always larger than the refractive index of the dielectric n_{d}, the bulk refractive index sensitivity of the effective index of the surface plasmon $(\delta n_{\mathrm{ef}}/\delta n)_{\mathrm{B}}$ is always larger than the sensitivity of a free space plane wave in the infinite dielectric medium (which is equal to one). For metals with a negative real part of the permittivity $\varepsilon'_{\mathrm{m}} < 0$ and a magnitude much larger than the imaginary part $\left|\varepsilon'_{\mathrm{m}}\right| \gg \varepsilon''_{\mathrm{m}}$, the sensitivity of the effective index of the surface plasmon to a bulk refractive change can be expressed as:

$$\left(\frac{\delta n_{\mathrm{ef}}}{\delta n}\right)_{\mathrm{B}} \doteq \left(\frac{\varepsilon'_{\mathrm{m}}}{\varepsilon'_{\mathrm{m}} + n_{\mathrm{d}}^2}\right)^{3/2}. \tag{58}$$

Equation 58 suggests that the sensitivity depends on the real part of the permittivity of the metal and decreases with its increasing magnitude. As the magnitude of the real part of the permittivity of gold decreases with an increasing wavelength (Fig. 3), the dependence of $(\delta n_{ef}/\delta n)_B$ on the wavelength follows the same trend, Fig. 15. For gold as a surface plasmon-supporting metal, both the results of the perturbation theory (Eq. 57) and its approximation (Eq. 58) agree very well with the rigorous approach based on the numerical calculation of the effective index of surface plasmon for the perturbed and unperturbed waveguide.

A change in the surface plasmon propagation constant induced by a surface refractive index change occurring within a layer with a thickness h can be calculated by substituting the perturbation of the permittivity profile Eq. 55 and the field distribution of the surface plasmon Eq. 48 into Eq. 53. After a straightforward mathematical manipulation we obtain:

$$\delta\beta = \frac{\beta^3}{2k^2\varepsilon_d^2}\left[1 - \exp(-2\gamma_d h)\right]\delta\varepsilon = \frac{\beta^3}{k^2 n_d^3}\left[1 - \exp(-2\gamma_d h)\right]\delta n\,, \tag{59}$$

where $\gamma_d = \sqrt{\beta^2 - \omega^2\mu_0\varepsilon_0\varepsilon_d}$ (a sign of the square root is selected so that $\mathrm{Re}\{\gamma_d\} > 0$). For the perturbation of the effective index of the surface plasmon, this equation yields:

$$\delta n_{ef} = \frac{\mathrm{Re}\left\{\beta^3\left[1 - \exp(-2\gamma_d h)\right]\right\}}{k^3 n_d^3}\delta n\,. \tag{60}$$

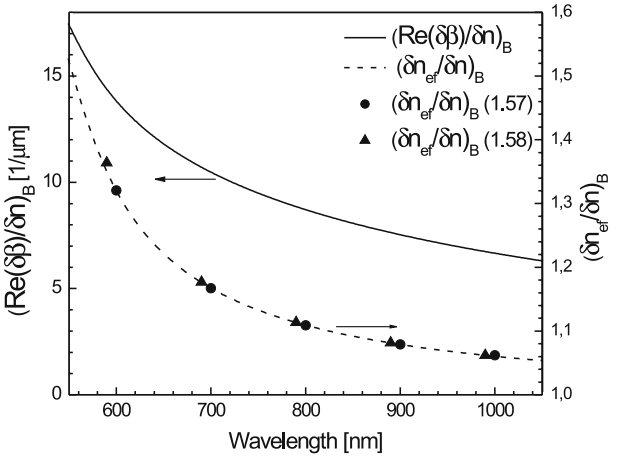

Fig. 15 Sensitivity of the real propagation constant (—) and effective index (- - -) of a surface plasmon on a metal–dielectric interface to a bulk refractive index change as a function of wavelength calculated rigorously from eigenvalue equation and using the perturbation theory. Waveguiding structure: gold–dielectric ($n_d = 1.32$)

The perturbation of the effective index of a surface plasmon depends exponentially on the thickness of the layer within which the refractive index change occurs. For a thicknesses much larger than the penetration depth of the surface plasmon ($h \gg L_{pd} = 1/\,\mathrm{Re}\,\{\gamma_d\}$), the exponential term can be neglected and Eq. 60 simplifies to Eq. 57. For refractive index changes occurring within a layer thinner than the penetration depth of the field of the surface plasmon ($h \ll L_{pd} = 1/\,\mathrm{Re}\,\{\gamma_d\}$), the expressions for the perturbations in the propagation constant and the effective refractive index can be reduced to:

$$\delta\beta = \frac{2\gamma_d\beta^3}{k^2 n_d^3} h\delta n\,, \tag{61}$$

$$\delta n_{ef} = \frac{2\,\mathrm{Re}\left\{\gamma_d\beta^3\right\}}{k^3 n_d^3} h\delta n\,. \tag{62}$$

Figure 16 shows the sensitivity of the propagation constant $(\mathrm{Re}(\delta\beta)/\delta n)_S$ and effective index $(\delta n_{ef}/\delta n)_S$ to a surface refractive index change calculated for a surface plasmon supported on gold and a refractive index change occurring within a 5 nm thick layer at the surface of the metal supporting a surface plasmon. As the layer thickness is much smaller than the penetration depth of the field of the surface plasmon on the considered structure, the sensitivity is a linear function of the thickness of the layer h.

If the real part of the permittivity of the metal is much larger than the imaginary part $\left|\varepsilon'_m\right| \gg \varepsilon''_m$, the sensitivity of the effective index of a surface

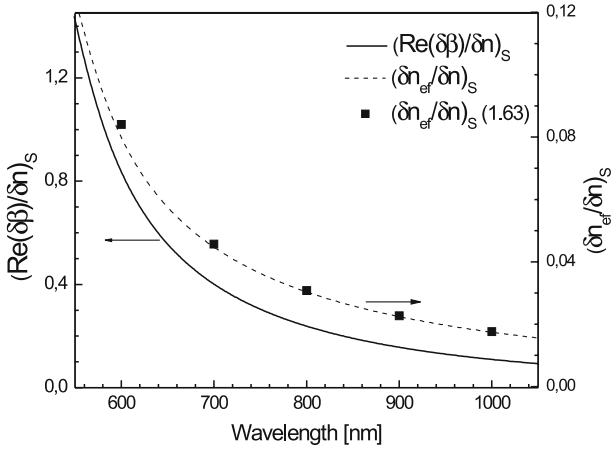

Fig. 16 Sensitivity of the propagation constant and effective index of a surface plasmon on a metal–dielectric interface to a surface refractive index change as a function of wavelength. Waveguiding structure: gold–thin dielectric film ($h = 5$ nm), dielectric superstrate ($n_d = 1.32$)

plasmon to a surface refractive index change can be expressed as:

$$\left(\frac{\delta n_{\mathrm{ef}}}{\delta n}\right)_{\mathrm{S}} = 2\frac{n_{\mathrm{ef}}^3}{n_{\mathrm{d}}^3}\frac{h}{L_{\mathrm{pd}}} = \left(\frac{\delta n_{\mathrm{ef}}}{\delta n}\right)_{\mathrm{B}}\frac{2h}{L_{\mathrm{pd}}}\,. \tag{63}$$

By employing the approximate expressions for the bulk refractive index sensitivity of the effective index Eq. 58 and low-loss metal approximation of L_{pd} (Eq. 48), Eq. 63 can be reduced to:

$$\left(\frac{\delta n_{\mathrm{ef}}}{\delta n}\right)_{\mathrm{S}} \doteq \left(\frac{\varepsilon'_{\mathrm{m}}}{\varepsilon'_{\mathrm{m}} + n_{\mathrm{d}}^2}\right)^{\frac{3}{2}} \frac{2n_{\mathrm{d}}^2}{\sqrt{-\varepsilon'_{\mathrm{m}} - n_{\mathrm{d}}^2}} hk\,. \tag{64}$$

As follows from Eq. 63, the sensitivity of the effective index to a surface refractive index change is proportional to the bulk refractive index sensitivity and the thickness of the layer within which the surface refractive index change occurs, and is inversely proportional to the penetration depth of the surface plasmon. As the penetration depth of a surface plasmon on gold increases with increasing wavelength, the surface refractive index sensitivity of the effective index (Fig. 16) decreases with the wavelength faster than the bulk refractive index sensitivity (Fig. 15). As illustrated in Fig. 16, the approximate equation for the sensitivity to as surface refractive index change (Eq. 63) yields results that are in a good agreement with the rigorous approach based on the numerical calculation of the effective index of surface plasmon for the perturbed and unperturbed waveguide from the appropriate eigenvalue equations.

3.2
Perturbed Surface Plasmons on Dielectric–Metal–Dielectric Waveguides

Perturbation of symmetric and antisymmetric surface plasmons (Sect. 2.2) propagating along a thin metal film with a thickness $2d$ can be calculated by determining the propagation constants of the surface plasmons supported by the unperturbed and perturbed waveguides as solutions to the eigenvalue (Eq. 35). The sensitivity of the effective index $(\delta n_{\mathrm{ef}}/\delta n)_{\mathrm{B}}$ to bulk refractive index changes in the superstrate as a function of metal layer thickness is shown in Fig. 17. For the considered structure and thicknesses of the metal film, the sensitivity of the antisymmetric surface plasmon is higher than that of its symmetric counterpart. The sensitivity of the symmetric surface plasmon increases with the thickness of the metal film, while the sensitivity of the antisymmetric surface plasmon follows an opposite trend. For thick metal films, the coupled surface plasmons consists of two weakly coupled surface plasmons propagating on opposite surfaces of the metal film and therefore the sensitivities of both the symmetric and antisymmetric surface plasmons

approach the value of one half of the sensitivity of the surface plasmon at a single metal–dielectric interface.

Figure 18 shows the sensitivity of the effective index $(\delta n_{\mathrm{ef}}/\delta n)_{\mathrm{B}}$ to bulk refractive index changes for symmetric and antisymmetric surface plasmons on a thin gold film. While the sensitivity of the effective index of the antisymmetric surface plasmon decreases with an increasing wavelength, sensitivity of its symmetric counterpart varies only slightly over the considered wavelength range.

The sensitivity of the effective index of the symmetric and antisymmetric surface plasmons to a surface refractive index change, Figs. 19 and 20, follows basically the same trends as the sensitivity to bulk refractive index changes.

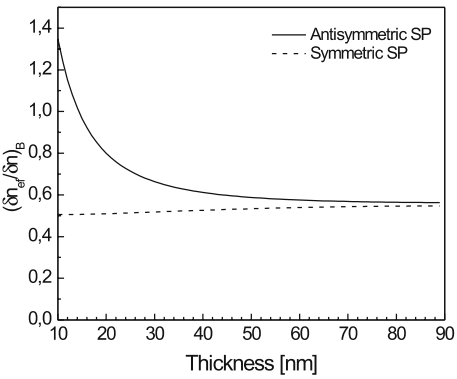

Fig. 17 Sensitivity of the effective index of symmetric and antisymmetric surface plasmons to bulk refractive index changes as a function of the thickness of metal layer. Waveguide configuration: dielectric ($n_1 = 1.32$)–gold ($\varepsilon_{\mathrm{m}} = -25 + 1.44\mathrm{i}$)–dielectric superstrate ($n_{\mathrm{d}} = 1.32$), wavelength 800 nm

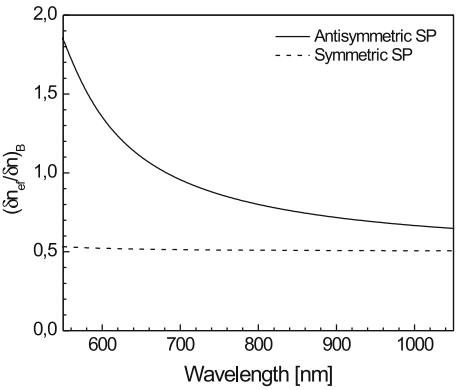

Fig. 18 Sensitivity of the effective index of symmetric and antisymmetric surface plasmons to bulk refractive index changes as a function of wavelength. Waveguide configuration: dielectric ($n_1 = 1.32$)–gold ($2d = 20$ nm)–dielectric superstrate ($n_{\mathrm{d}} = 1.32$)

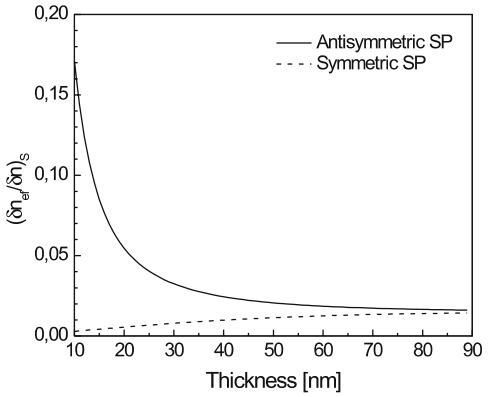

Fig. 19 Sensitivity of the effective index of symmetric and antisymmetric surface plasmons to surface refractive index changes as a function of the thickness of metal film. Waveguide configuration: dielectric ($n_1 = 1.32$)–gold ($\varepsilon_m = -25 + 1.44i$)–thin dielectric film ($h = 5$ nm), dielectric superstrate ($n_d = 1.32$), wavelength 800 nm

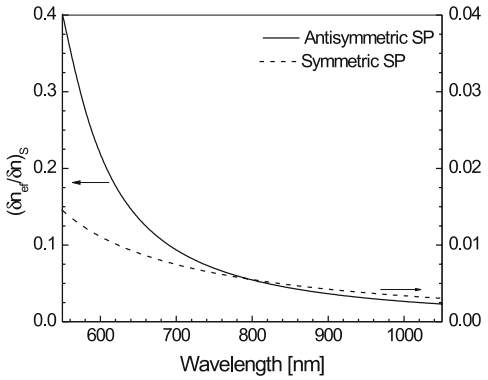

Fig. 20 Sensitivity of the effective index of symmetric and antisymmetric surface plasmons to surface refractive index changes as a function of wavelength. Waveguide configuration: dielectric ($n_1 = 1.32$)–gold ($2d = 20$ nm)–thin dielectric film ($h = 5$ nm), dielectric superstrate ($n_d = 1.32$)

4 Excitation of Surface Plasmons

4.1 Prism Coupling

The most common approach to excitation of surface plasmons is by means of a prism coupler and the attenuated total reflection method (ATR). There are two configurations of the ATR method – Kretschmann geometry [5] and

Otto geometry [4]. In the Kretschmann geometry of the ATR method, a high refractive index prism with refractive index n_p is interfaced with a metal–dielectric waveguide consisting of a thin metal film with permittivity ε_m and thickness q, and a semi-infinite dielectric with a refractive index $n_d (n_d < n_p)$, Fig. 21.

When a light wave propagating in the prism is made incident on the metal film a part of the light is reflected back into the prism and a part propagates in the metal in the form of an inhomogeneous electromagnetic wave [13]. This inhomogeneous wave decays exponentially in the direction perpendicular to the prism–metal interface and is therefore referred as to an evanescent wave. If the metal film is sufficiently thin (less than 100 nm for light in visible and near infrared part of spectrum), the evanescent wave penetrates through the metal film and couples with a surface plasmon at the outer boundary of the metal film. The propagation constant of the surface plasmon propagating along a thin metal film β^{SP} is influenced by the presence of the dielectric on the opposite side of the metal film and can be expressed as

$$\beta^{SP} = \beta^{SP_0} + \Delta\beta = \frac{\omega}{c}\sqrt{\frac{\varepsilon_d \varepsilon_m}{\varepsilon_d + \varepsilon_m}} + \Delta\beta\,, \tag{65}$$

where β^{SP_0} is the propagation constant of the surface plasmon propagating along the metal–dielectric waveguide in the absence of the prism and $\Delta\beta$ accounts for the finite thickness of the metal film and the presence of the prism. In order for the coupling between the evanescent wave and the surface plasmon to occur, the propagation constant of the evanescent wave β^{EW} and that of the surface plasmon β^{SP} have to be equal:

$$\frac{2\pi}{\lambda} n_p \sin\theta = k_z = \beta^{EW} = \mathrm{Re}\left\{\beta^{SP}\right\} = \mathrm{Re}\left\{\frac{2\pi}{\lambda}\sqrt{\frac{\varepsilon_d \varepsilon_m}{\varepsilon_d + \varepsilon_m}} + \Delta\beta\right\}. \tag{66}$$

In terms of effective index, this coupling condition can be written as follows:

$$n_p \sin\theta = n_{ef}^{EW} = n_{ef}^{SP} = \mathrm{Re}\left\{\sqrt{\frac{\varepsilon_d \varepsilon_m}{\varepsilon_d + \varepsilon_m}}\right\} + \Delta n_{ef}^{SP}\,, \tag{67}$$

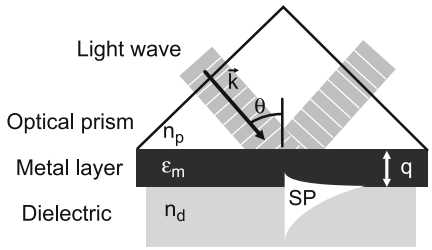

Fig. 21 Excitation of surface plasmons in the Kretschmann geometry of the attenuated total reflection (ATR) method

where n_{ef}^{EW} is the effective index of the evanescent wave, n_{ef}^{SP} is the effective index of the surface plasmon, and $\Delta n_{ef}^{SP} = \mathrm{Re}\{\Delta\beta\lambda/2\pi\}$. The coupling condition between the light wave and the surface plasmon is illustrated in Fig. 22, which shows the spectral dependencies of effective indices of a surface plasmon on a gold–water interface and an evanescent light wave produced by a light wave incident on the gold film from a BK7 glass prism. For each wavelength, the matching condition is satisfied for a single angle of incidence, the coupling angle, which increases with decreasing wavelength.

In the Otto geometry, a high refractive index prism with refractive index n_p is interfaced with a dielectric–metal waveguide consisting of a thin dielectric film with refractive index $n_d (n_d < n_p)$ and thickness q, and a semi-infinite metal with permittivity ε_m, Fig. 23.

In Otto geometry, a light wave incident on the prism–dielectric film interface at an angle of incidence larger than the critical angle of incidence for these two media produces an evanescent wave propagating along the interface between the prism and the dielectric film. If the thickness of the dielectric layer is chosen properly (typically few microns), the evanescent wave and a surface plasmon at the dielectric–metal interface can couple. For the coupling to occur, the propagation constant of the evanescent wave and that of the surface plasmon have to be equal.

The attenuated total reflection method can be also used to excite coupled surface plasmons on thin metal films. The coupling of a light into a symmetric or antisymmetric surface plasmon supported by a thin film (Sect. 2.2) can be in principle achieved in a geometry similar to the Otto geometry (Fig. 23) in which the semi-infinite metal is replaced by a thin metal film [20].

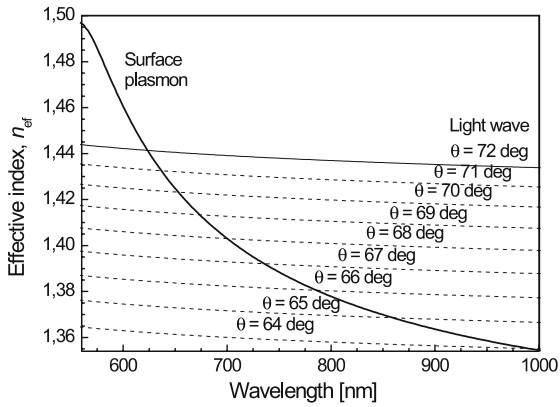

Fig. 22 Spectral dependence of the effective index of a surface plasmon on the interface of gold–water and the effective index of the evanescent light wave produced by a plane light wave incident on the gold film from an optical prism (BK 7 glass) under nine different angles of incidence

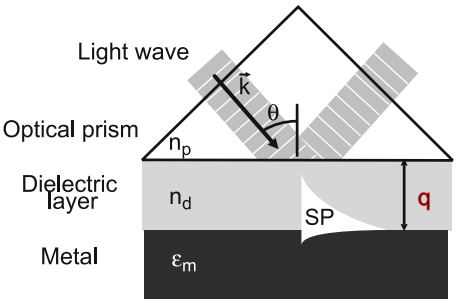

Fig. 23 Excitation of surface plasmons in the Otto geometry of the attenuated total reflection (ATR) method

The interaction between a light wave and a surface plasmon in the ATR method can be investigated using the Fresnel multilayer reflection theory [18]. Herein, we shall present analysis of the reflectivity for the Kretschmann geometry of the ATR method.

Assuming an incident plane wave and a structure prism–metal–dielectric infinite in the *y*-*z* plane (Fig. 24), the amplitude of reflected light A_R can be expressed as:

$$A_R = r_{pmd} A_I = \left| r_{pmd} \right| e^{i\phi} A_I \,, \tag{68}$$

where A_I is the amplitude of the incident light wave, r_{pmd} is an amplitude reflection coefficient and ϕ is a phase shift. The amplitude reflection coefficient is:

$$r_{pmd} = \frac{r_{pm} + r_{md} \exp(2ik_{mx}q)}{1 + r_{pm} r_{md} \exp(2ik_{mx}q)} \,, \tag{69}$$

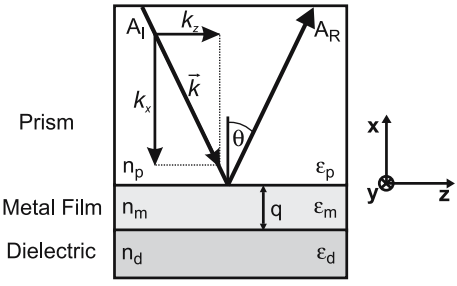

Fig. 24 Light reflection in the Kretschmann geometry of the ATR method

where:

$$k_{ix} = \sqrt{\left(\frac{2\pi}{\lambda}\right)^2 \varepsilon_i - k_z^2}\,, \tag{70}$$

$$r_{ij} = \frac{\varepsilon_j k_{ix} - \varepsilon_i k_{jx}}{\varepsilon_j k_{ix} + \varepsilon_i k_{jx}} \quad \text{for the TM polarization}\,, \tag{71}$$

$$r_{ij} = \frac{k_{ix} - k_{jx}}{k_{ix} + k_{jx}} \quad \text{for the TE polarization}\,, \tag{72}$$

and where subscripts i and j are p, m, or d [19]. Reflectivity (power reflection coefficient) of the structure R is then:

$$R = \left|r_{\mathrm{pmd}}\right|^2\,. \tag{73}$$

Figure 25 shows typical dependencies of the reflectivity and phase on the angle of incidence calculated for four different thicknesses of the metal film.

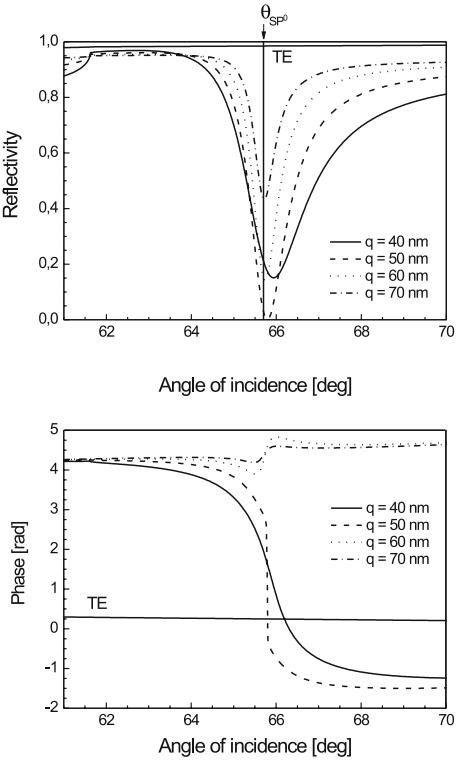

Fig. 25 Reflectivity (*upper plot*) and phase shift (*lower plot*) as a function of the angle of incidence for four different thicknesses of the metal film and TM polarization. Configuration: BK7 glass ($n_\mathrm{p} = 1.51$), gold film ($\varepsilon_\mathrm{m} = -25 + 1.44\mathrm{i}$), water ($n_\mathrm{d} = 1.329$), wavelength 800 nm, reflectivity and phase of the TE polarization are shown for comparison

The angular reflectivity spectra exhibit distinct dips that are associated with the transfer of energy from the incident light wave into a surface plasmon and its subsequent dissipation in the metal film (Fig. 25, upper plot). The interaction between the incident light wave and the surface plasmon also affects the phase of the reflected light, which exhibits an abrupt phase jump [20] (Fig. 25, lower plot). Angular dependencies of the reflectivity and phase of the TE-polarized light contain no resonant features, as no guided modes can be excited by the TE-polarized light in this geometry.

As follows from Fig. 25 (upper plot), the resonant angle of incidence decreases with an increasing metal film thickness and approaches the value θ_{SP_0} corresponding to the coupling of light to a surface plasmon propagating along an isolated metal–dielectric waveguide (Eq. 65, $q \to \infty$, $\Delta\beta = 0$). The depth of the reflectivity dip depends on the thickness of the metal film. The strongest excitation of a surface plasmon ($R = 0$) occurs for a single metal film thickness (for the considered geometry and wavelength, the optimum coupling thickness was about 50 nm). The width and asymmetry of the reflectivity dip increase with a decreasing metal film thickness.

Assuming that the permittivity of metal ε_{m} obeys $\left|\varepsilon'_{\mathrm{m}}\right| \gg n_{\mathrm{d}}$ and $\left|\varepsilon'_{\mathrm{m}}\right| \gg \varepsilon''_{\mathrm{m}}$, the reflectivity Eq. 69 can be expanded around the resonant value of k_z yielding a Lorentzian (with respect to k_z) approximation of the reflectivity [6]:

$$R(k_z) \doteq 1 - \frac{4\,\mathrm{Im}\left\{\beta^{\mathrm{SP}_0}\right\}\mathrm{Im}\left\{\Delta\beta\right\}}{\left[k_z - \mathrm{Re}\left\{\beta^{\mathrm{SP}}\right\}\right]^2 + \left(\mathrm{Im}\left\{\beta^{\mathrm{SP}_0}\right\} + \mathrm{Im}\left\{\Delta\beta\right\}\right)^2}\,, \tag{74}$$

where:

$$\beta^{\mathrm{SP}} = \beta^{\mathrm{SP}_0} + \Delta\beta\,, \tag{75}$$

$$\beta^{\mathrm{SP}_0} = \frac{\omega}{c}\sqrt{\frac{\varepsilon_{\mathrm{d}}\varepsilon_{\mathrm{m}}}{\varepsilon_{\mathrm{d}} + \varepsilon_{\mathrm{m}}}}\,, \tag{76}$$

$$\Delta\beta = r_{\mathrm{pm}}\,\mathrm{e}^{2\mathrm{i}k_{zm}q}2\frac{\omega}{c}\left(\frac{\varepsilon_{\mathrm{d}}\varepsilon_{\mathrm{m}}}{\varepsilon_{\mathrm{d}} + \varepsilon_{\mathrm{m}}}\right)^{3/2}\frac{1}{\varepsilon_{\mathrm{d}} - \varepsilon_{\mathrm{m}}}\,. \tag{77}$$

The term $\Delta\beta$ describes the effect of the prism and, as a complex quantity, has a real part, which perturbs the real part of the propagation constant of a surface plasmon on the interface of semi-infinite dielectric and metal, and an imaginary part, which causes an additional damping of the surface plasmon due to the outcoupling of a portion of the field into the prism [6]. In terms of effective index, the reflectivity (Eq. 74) can be rewritten as follows:

$$R(\theta, \lambda) \doteq 1 - \frac{4\gamma_i\gamma_{\mathrm{rad}}}{(n_{\mathrm{p}}\sin\theta - n_{\mathrm{ef}}^{\mathrm{SP}})^2 + (\gamma_i + \gamma_{\mathrm{rad}})^2}\,, \tag{78}$$

where $\gamma_i = \mathrm{Im}\left\{\beta^{\mathrm{SP}_0}\right\}\lambda/2\pi$ and $\gamma_{\mathrm{rad}} = \mathrm{Im}\left\{\Delta\beta\right\}\lambda/2\pi$. As follows from Eq. 78, the dip in the reflectivity spectrum is centered at the angle of incidence de-

scribed by the coupling condition Eq. 67 with $\Delta\beta$ given by Eq. 77. Figure 26 shows the angular reflectivity calculated using the rigorous approach (Eq. 69) and the Lorentzian approximation (Eq. 78) with the propagation constant of a surface plasmon approximated by β^{SP_0} for a model structure: BK7 glass prism, gold film, and water. The approximation provides a good estimate of the position of the reflectivity dip (which would be even closer if the term $\Delta\beta$ was not neglected) and predicts well the shape of the reflectivity curve in the neighborhood of the minimum. In addition, the Lorentzian curve exhibits approximately the same width as the dips calculated using the rigorous approach.

The coupling strength and subsequently the depth of the dip reach the maximum if the radiation and absorption losses of a surface plasmon are equal: $\gamma_i = \gamma_{rad} = \gamma$. As γ_{rad} decreases with an increasing metal film thickness (as can be deduced from Eq. 77), the condition $\gamma_i = \gamma_{rad}$ is satisfied only for a single thickness of the metal film, as predicted by the Fresnel reflection theory (Fig. 25). The optimum coupling metal thickness depends on the wavelength and materials involved. For a gold film and wavelengths between 600 and 1000 nm, the optimum coupling thickness varies between 44 nm and 50 nm.

When the optimum coupling occurs ($\gamma_i = \gamma_{rad} = \gamma$), the angular half-width of the dip $\Delta\theta_{1/2}$ (angular width of the dip at $R = 0.5$) can be expressed from Eq. 78 as:

$$\Delta\theta_{1/2} = \frac{4\gamma}{n_p \cos\theta}, \tag{79}$$

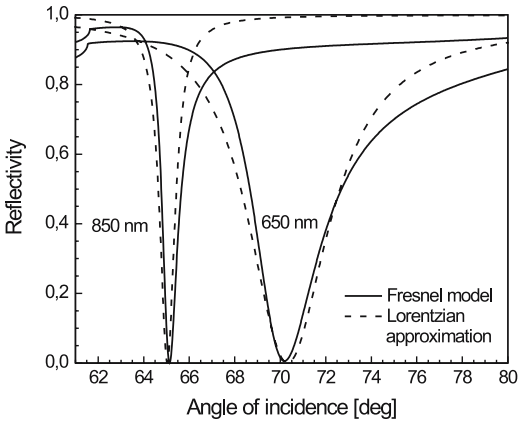

Fig. 26 TM reflectivity as a function of angle of incidence calculated for two different wavelengths using the rigorous Fresnel reflection theory and its Lorentzian approximation. Configuration: BK7 glass, gold film (thickness 48 nm for wavelength 650 nm, and 50 nm for wavelength 850 nm), water

where θ denotes the coupling angle. Equation 79 suggests that the angular width of the dip is proportional to the attenuation of the surface plasmon. As the attenuation coefficient γ decreases rapidly with an increasing wavelength, while the factor $\cos\theta$ changes with the wavelength only slowly, reflectivity dips associated with the excitation of surface plasmons at longer wavelengths (and smaller angles of incidence) are narrower than the dips associated with the excitation of surface plasmons at shorter wavelengths (and higher angles of incidence), Fig. 26.

The characteristic absorption dip can be observed not only in the angular domain, but also when the angle of incidence is kept constant and the wavelength is varied, Fig. 27.

The spectral reflectivity is also described by Eqs. 69 and 74. For low-loss metals ($\left|\varepsilon'_{\mathrm{m}}\right| \gg \varepsilon''_{\mathrm{m}}$) with a large real part of the permittivity ($\left|\varepsilon'_{\mathrm{m}}\right| \gg \varepsilon_{\mathrm{d}}$), the spectral half-width of the dip $\Delta\lambda_{1/2}$ for the optimum coupling ($\gamma_i = \gamma_{\mathrm{rad}} = \gamma$)

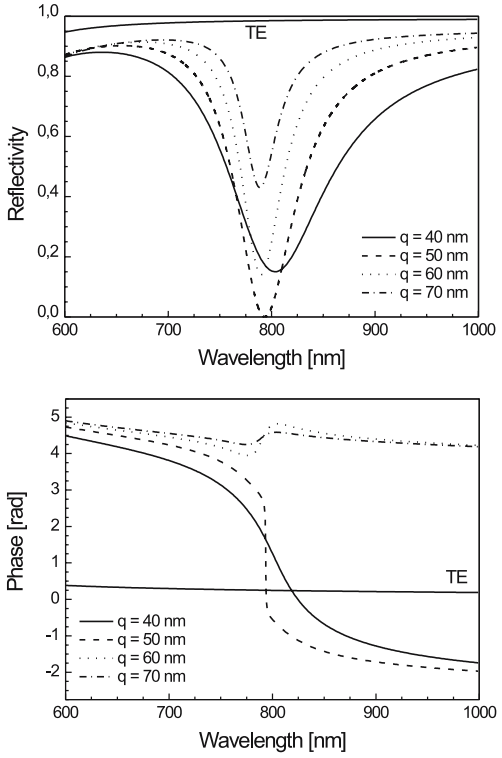

Fig. 27 Reflectivity (*upper plot*) and phase (*lower plot*) of reflected light as a function of wavelength for four different thicknesses of the metal film. Configuration: BK7 glass, gold film, water, angle of incidence 66 deg. Reflectivity and phase for TE polarization are given for comparison

can be calculated from Eq. 74 as:

$$\Delta\lambda_{1/2} = \frac{4\gamma}{\left| \frac{dn_p}{d\lambda} \sin\theta - \frac{dn_{ef}^{SP}}{d\lambda} \right|}, \tag{80}$$

where $dn_p/d\lambda$ is the dispersion of the prism and $dn_{ef}^{SP}/d\lambda$ is the dispersion of the effective index of the surface plasmon. While the attenuation coefficient γ_i decreases with an increasing wavelength, the difference in dispersions

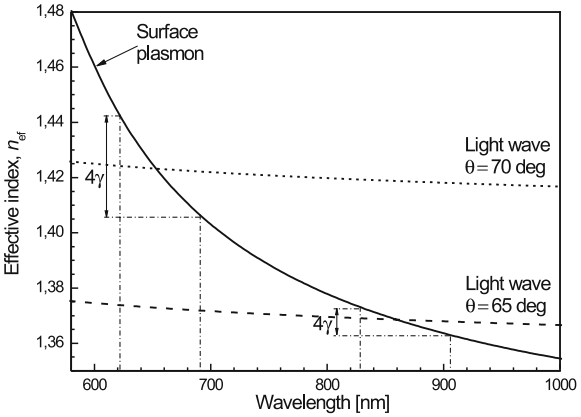

Fig. 28 Spectral dependence of the effective refractive index of a surface plasmon on gold–water interface and the effective index of the evanescent light wave produced in a gold film by a plane light wave incident on the gold film from a BK7 glass prism under two different angles of incidence

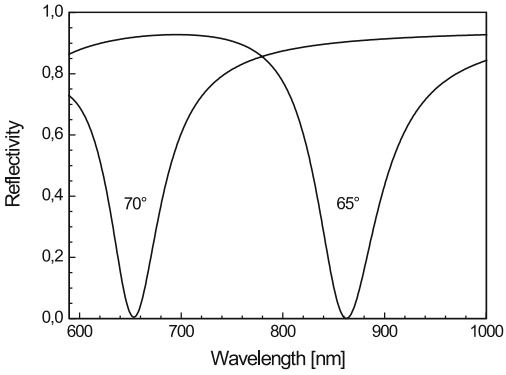

Fig. 29 TM reflectivity as a function of wavelength calculated for two different angles of incidence using the rigorous Fresnel reflection theory. Configuration: BK7 glass, gold film (thickness 48 nm for the wavelength of 650 nm and 50 nm for the wavelength of 850 nm), water

of the effective indices of the evanescent wave and the surface plasmon decreases (Fig. 28) and therefore these two effects can compensate each other. This phenomenon is illustrated in Fig. 29, which shows reflectivity dips produced by the excitation of surface plasmons at the wavelengths of 650 and 850 nm. These dips exhibit approximately the same width although γ_i is about five times larger at the wavelength of 650 nm than at 850 nm.

4.2 Grating Coupling

Another approach to optical excitation of surface plasmons is based on the diffraction of light on a diffraction grating. In this method, a light wave is incident from a dielectric medium with the refractive index n_d on a metal grating with the dielectric constant ε_m, the grating period Λ and the grating depth q, Fig. 30.

When a light wave with the wavevector $\boldsymbol{k}$ is made incident on the surface of the grating, diffraction gives rise to a series of diffracted waves. The wavevector of the diffracted light $\boldsymbol{k}_m$ is:

$$\boldsymbol{k}_m = \boldsymbol{k} + m\boldsymbol{G}\,, \tag{81}$$

where m is an integer and denotes the diffraction order and G is the grating vector [21]. The grating vector lies in the plane of the grating (plane y-z in Fig. 30) and is perpendicular to the grooves of the grating. Its magnitude is inversely proportional to the pitch of the grating and therefore, for the grating geometry considered herein, it can be expressed as:

$$\boldsymbol{G} = \frac{2\pi}{\Lambda}\boldsymbol{z}_0\,. \tag{82}$$

Therefore the component of the wavevector of the diffracted light perpendicular to the plane of the grating k_{xm} is equal to that of the incident wave while the component of the wavevector in the plane of the grating k_{zm} is diffraction altered:

$$k_{zm} = k_z + m\frac{2\pi}{\Lambda}\,. \tag{83}$$

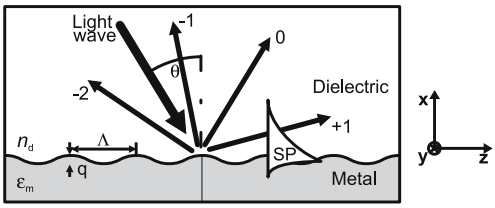

Fig. 30 Excitation of surface plasmons by the diffraction of light on a diffraction grating

The diffracted waves can couple with a surface plasmon when the propagation constant of the diffracted wave propagating along the grating surface k_{zm} and that of the surface plasmon β^{SP} are equal:

$$\frac{2\pi}{\lambda} n_{\mathrm{d}} \sin\theta + m\frac{2\pi}{\Lambda} = k_{zm} = \pm \operatorname{Re}\left\{\beta^{\mathrm{SP}}\right\} , \tag{84}$$

where:

$$\beta^{\mathrm{SP}} = \beta^{\mathrm{SP}_0} + \Delta\beta = \frac{\omega}{c}\sqrt{\frac{\varepsilon_{\mathrm{d}}\varepsilon_{\mathrm{m}}}{\varepsilon_{\mathrm{d}} + \varepsilon_{\mathrm{m}}}} + \Delta\beta , \tag{85}$$

and β^{SP_0} denotes the propagation constant of the surface plasmon propagating along the smooth interface of a semi-infinite metal and a semi-infinite dielectric, and $\Delta\beta$ accounts for the presence of the grating. In terms of effective index, the coupling condition can be rewritten as:

$$n_{\mathrm{d}} \sin\theta + m\frac{\lambda}{\Lambda} = \pm\left(\operatorname{Re}\left\{\sqrt{\frac{\varepsilon_{\mathrm{d}}\varepsilon_{\mathrm{m}}}{\varepsilon_{\mathrm{d}} + \varepsilon_{\mathrm{m}}}}\right\} + \Delta n_{\mathrm{ef}}^{\mathrm{SP}}\right) , \tag{86}$$

where $\Delta n_{\mathrm{ef}}^{\mathrm{SP}} = \operatorname{Re}\{\Delta\beta\lambda/2\pi\}$.

The coupling condition between a diffracted light wave and a surface plasmon is illustrated in Fig. 31. The effective index of light diffracted on two different gratings ($\Lambda = 540$ nm and $\Lambda = 672$ nm) is diffraction enhanced to match the effective index of a surface plasmon on a gold–water interface. As illustrated in Fig. 31, different orders of diffraction (first order for the grating with $\Lambda = 672$ nm and minus first order for the grating with $\Lambda = 540$ nm) can be used to fulfill the matching condition. The effective index of the inhomoge-

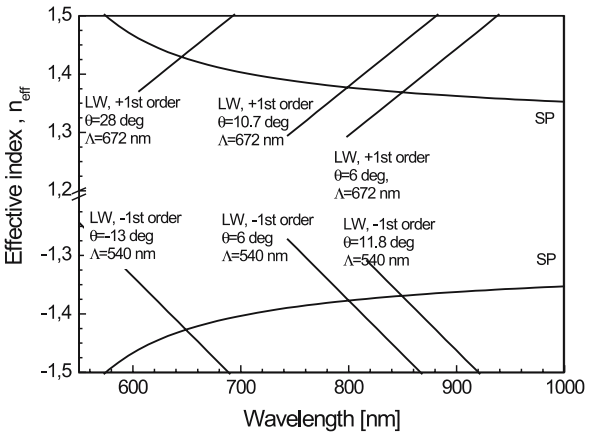

Fig. 31 Spectral dependence of the effective index of a surface plasmon on gold–water interface and the effective index of the light wave produced by a diffraction of light on a diffraction grating calculated for two different grating periods and three different angles of incidence

neous light wave is approximately a linear function of wavelength with a slope equal to m/Λ, which is positive for $m > 0$ and negative for $m < 0$. The coupling condition Eq. 86 can be fulfilled for various combinations of the angle of incidence, grating pitch, and diffraction order. For the positive diffraction orders, the coupling wavelength increases with a decreasing angle of incidence, while for the negative diffraction orders, the coupling wavelength increases with an increasing angle of incidence.

The grating-moderated interaction between a light wave and a surface plasmon can be investigated by solving Maxwell's equations in differential or integral form. In the differential method, the grating profile is approximated with a stack of layers in which a solution of the Maxwell equations is calculated in the form of a Rayleigh series and the total solution of the diffraction problem is found by applying boundary conditions at each interface [22, 23]. The integral method assumes a certain current flow at the grating surface

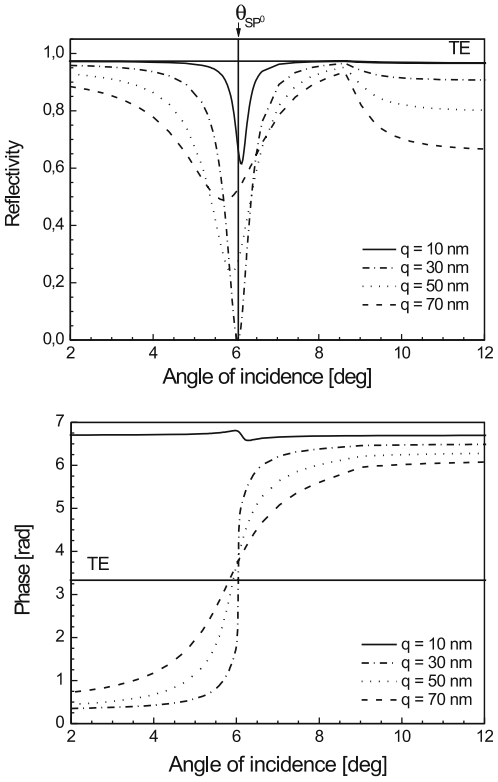

Fig. 32 Reflectivity (*upper plot*) and phase (*lower plot*) as a function of the angle of incidence for four different depths of a metallic sinusoidal grating and TM polarization. Configuration: gold ($\varepsilon_m = -25 + 1.44i$), water ($n_d = 1.329$), wavelength 800 nm, grating period 540 nm, angle of incidence taken in air. Reflectivity and phase of the TE polarization are shown for comparison

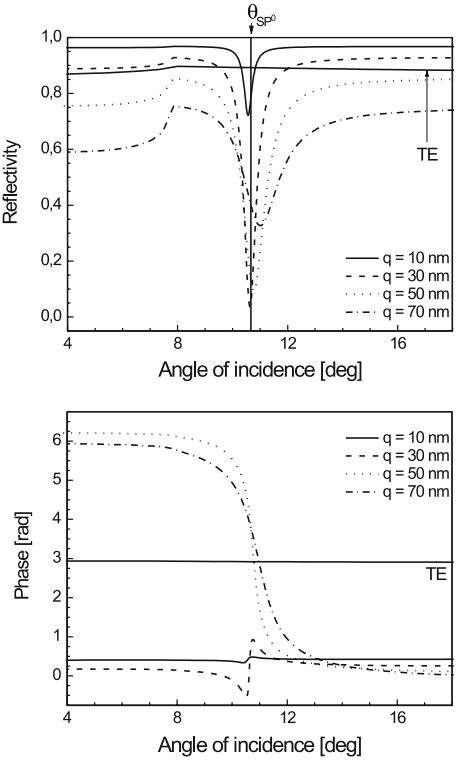

Fig. 33 Reflectivity (*upper plot*) and phase (*lower plot*) as a function of the angle of incidence for four different depths of metallic sinusoidal grating and TM polarization. Configuration: gold ($\varepsilon_m = -25 + 1.44i$), water ($n_d = 1.329$), wavelength 800 nm, grating period 672 nm, angle of incidence taken in air. Reflectivity and phase of the TE polarization are shown for comparison

and reduces the problem to the calculation of the Helmholtz–Kirchhoff integral [24]. Figures 32 and 33 show the dependence of the reflectivity and phase on the angle of incidence for light incident from water onto a gold grating and two different grating pitches, $\Lambda = 540$ nm (Fig. 32) and $\Lambda = 672$ nm (Fig. 33), and four different grating depths. These spectra were calculated using the integral method. The angular reflectivity spectra (upper plots in Fig. 32 and Fig. 33) exhibits a characteristic dip caused by the transfer of energy of the incident light into a surface plasmon. On shallow diffraction gratings, surface plasmons are excited at the angles of incidence close to the coupling angles predicted from the matching condition, neglecting the effect of the grating ($q \to 0$ and $\Delta n_{ef}^{SP} = \mathrm{Re}\{\Delta\beta\} = 0$), Fig. 31. The coupling angle of incidence decreases with an increasing depth of the grating when the surface plasmons are excited by a negative order of diffraction, and follows an opposite trend when the surface plasmons are excited by a positive order of diffraction. The depth

of the reflectivity dip depends on the depth of the grating and the strongest excitation of a surface plasmon ($R = 0$) occurs for a single depth of the grating (for the considered geometry and wavelength, the optimum grating depth is about 30 nm). The width and asymmetry of the reflectivity dip increase with an increasing depth of grating. The interaction between the light wave and the surface plasmon results also in a change in the phase of the reflected light, Fig. 32 and Fig. 33 (lower plot).

The characteristic absorption dip can be observed not only in the angular domain, but also when the angle of incidence is kept constant and the wavelength is varied, as illustrated in Fig. 34 and Fig. 35.

Figure 36 shows the angular reflectivity for light incident from water onto a gold grating. The dips produced at the wavelength of 850 nm are about five times narrower than those occurring at 650 nm. The ratio of the dip widths corresponds to the ratio of the attenuation coefficients for surface plasmons

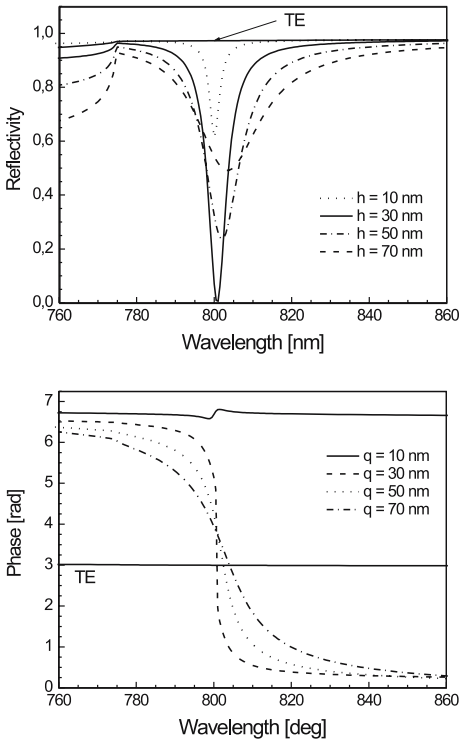

Fig. 34 Reflectivity (*upper plot*) and phase (*lower plot*) as a function of the wavelength for four different modulation depths of metallic sinusoidal grating and TM polarization. Configuration: gold–water, angle of incidence 6 degrees, grating period 540 nm, angle of incidence taken in air. Reflectivity and phase of the TE polarization are shown for comparison

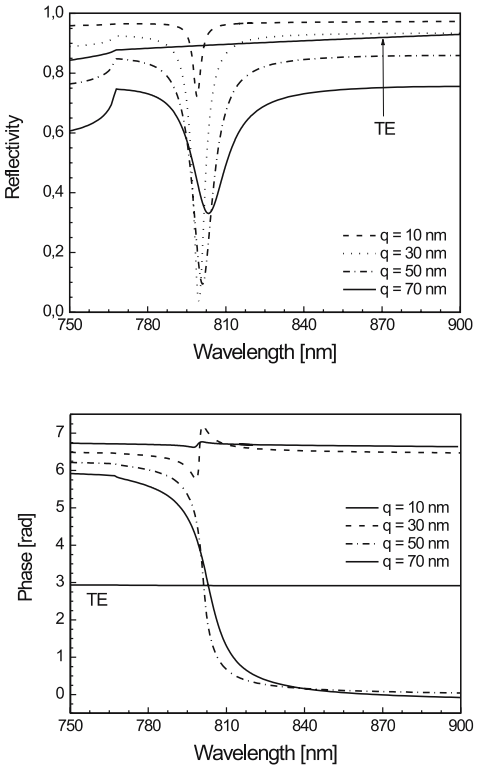

Fig. 35 Reflectivity (*upper plot*) and phase (*lower plot*) as a function of the wavelength for four different modulation depths of metallic sinusoidal grating and TM polarization. Configuration: gold–water, angle of incidence 10.7 degrees, grating period 672 nm, angle of incidence taken in air. Reflectivity and phase of the TE polarization are shown for comparison

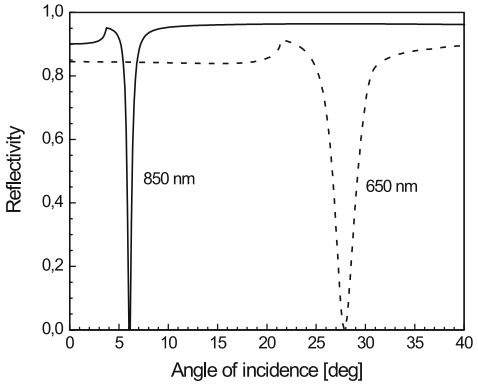

Fig. 36 Reflectivity as a function of angle of incidence calculated for two wavelengths. Configuration: gold–water interface, grating period 672 nm, angle of incidence taken in air

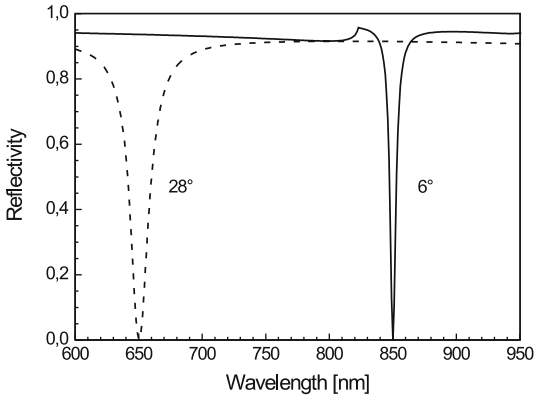

Fig. 37 Reflectivity as a function of wavelength calculated for two different angles of incidence. Configuration: gold–water interface, grating period 672 nm, angle of incidence taken in air

at 650 and 850 nm, as in the case of prism coupling (Sect. 4.1). However, the width of the dips observed in the wavelength spectrum (Fig. 37) varies with the wavelength, which contrasts with the weak dependence of the width of spectral dips in the case of prism coupling. This effect can be attributed to the fact that the difference in the dispersions of the effective indices of the evanescent wave and surface plasmon is large (Fig. 31) and varies relatively little over the considered wavelength range.

4.3 Waveguide Coupling

Surface plasmons can be also excited by modes of a dielectric waveguide. An example of a waveguiding structure integrating a dielectric waveguide and a metal–dielectric waveguide is shown in Fig. 38. A mode of the dielectric waveguide propagates along the waveguide and when it enters the region with

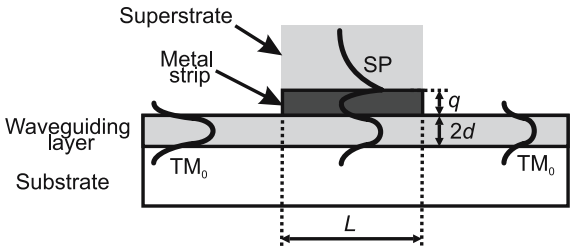

Fig. 38 Excitation of surface plasmons by a mode of a dielectric waveguide

a thin metal film, it penetrate through the metal film and couples with a surface plasmon at the outer boundary of the metal.

The coupling between the waveguide mode and a surface plasmon can occur when the propagation constant of the mode β_M is equal to the real part of the propagation constant of the surface plasmon β_{SP}:

$$\beta_M = \mathrm{Re}\{\beta_{SP}\} \ . \tag{87}$$

The coupling between the waveguide mode and a surface plasmon can be investigated by analyzing hybrid modes, which are solutions of the vector wave (Eq. 18) for the coupled waveguides [25]. The propagation of light through the entire waveguiding structure can be simulated using the mode expansion and propagation method [26]. In this method, the simulated waveguide is subdivided into longitudinally uniform sections and, in each section, a set of eigenmodes is calculated. The mutual relationships among modal amplitudes at both sides of the interface between the longitudinal sections are obtained from the continuity of the transversal field components by mode matching [26].

As surface plasmons are typically much more dispersive than modes of common dielectric waveguides, the coupling condition Eq. 87 is fulfilled only for a narrow range of wavelengths. Therefore, the excitation of a surface plasmon can be observed as a narrow dip in the spectrum of transmitted light, Fig. 39. The strength of the coupling depends on the metal thickness (Fig. 39) and the length of the interaction region (Fig. 40). The effect of the metal film thickness and interaction length is depicted in Figs. 39 and 40 for a model structure consisting of substrate (refractive index 1.514), a waveguiding layer (refractive index 1.517, thickness 3 μm), a thin gold layer, and superstrate (refractive index 1.40).

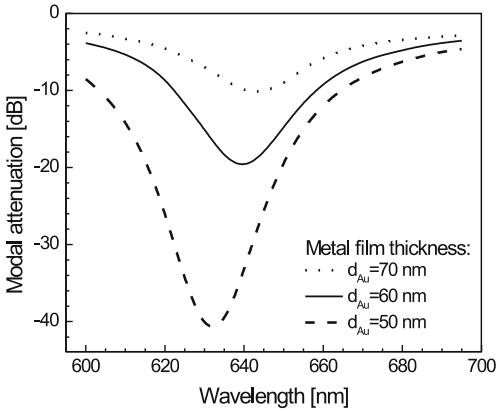

Fig. 39 Spectral dependence of the transmission of a slab waveguide with a thin metal strip for different thicknesses of the metal film, metal strip length $L = 1$ mm

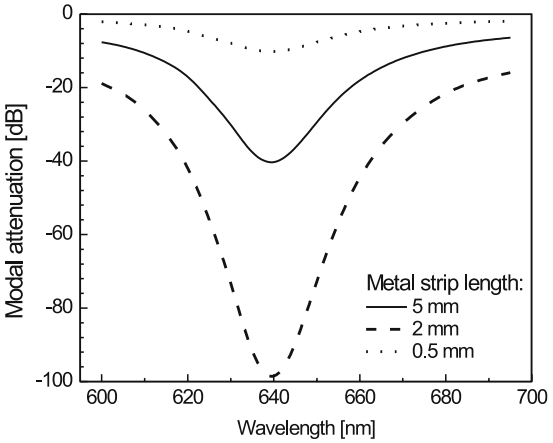

Fig. 40 Spectral dependence of the transmission of a slab waveguide with a thin metal strip for different lengths of the metal strip, metal film thickness $q = 60$ nm

5 Summary

Surface plasmons are special modes of electromagnetic field in metal–dielectric waveguides. They are characterized by the field distribution and complex propagation constant, which can be determined from an appropriate eigenvalue equation. The propagation constant of surface plasmons is highly sensitive to changes in the refractive index distribution, as can be demonstrated using the perturbation theory. Surface plasmons can be excited by light waves using (i) prism coupling and the attenuated total reflection, (ii) diffraction on a metal diffraction grating, and (iii) coupling among parallel optical waveguides.

References

1. Wood RW (1902) Philosophical Magazine 4:396
2. Fano U (1941) J Opt Soc Am 31:231
3. Turbadar T (1959) Proc Phys Soc 73:40
4. Otto A (1968) Zeits Phys 216:398
5. Kretschmann E, Raether H (1968) Z Naturforsch 2135–2136:2135–2136
6. Raether H (1988) Springer Tracts Mod Phys 111:1
7. Boardman AD (1982) Electromagnetic surface modes. Wiley, Chichester
8. Pockrand I, Swalen JD, Gordon JG, Philpott MR (1978) Surf Sci 74:237
9. Gordon JG, Ernst S (1980) Surf Sci 101:499
10. Snyder AW, Love JD (1983) Optical waveguide theorie, Chap viii. Science paperbacks 190. Chapman and Hall, London New York, p 734
11. Marcuse D (1973) Integrated optics. IEEE Press, New York

12. Marcuse D (1974) Theory of dielectric optical waveguides. Academic, New York
13. Born M, Wolf E (1999) Principles of optics: electromagnetic theory of propagation, interference and diffraction of light. Cambridge University Press, Cambridge
14. Palik ED, Ghosh G (1998) Handbook of optical constants of solids. Academic, San Diego
15. Stegeman GI, Burke JJ, Hall DG (1983) Optics Lett 8:383
16. Burke JJ, Stegeman GI, Tamir T (1986) Phys Rev B 33:5186
17. Sarid D (1981) Phys Rev Lett 47:1927
18. Tobiška P (2005) PhD Dissertation, Charles University, Prague
19. Yariv A, Yeh P (2003) Optical waves in crystals: propagation and control of laser radiation. Wiley, Hoboken NJ
20. Deck RT, Sarid D, Olson GA, Elson JM (1983) Appl Opt 22:3397
21. Grigorenko AN, Nikitin PI, Kabashin AV (1999) Appl Phys Lett 75:3917
22. Hutley MC (1982) Diffraction gratings. Academic, London
23. Moharam MG, Gaylord TK (1986) J Opt Soc Am A 3:1780
24. Li LF (1993) J Opt Soc Am A 10:2581
25. Goray LI, Seely JF (2002) Appl Opt 41:1434
26. Homola J (1997) Sens Act B Chem 39:286
27. Čtyroký J, Homola J, Skalský M (1997) Opt Quant Electron 29:301